ISSN 1028-8546

Volume XX, Number 4
Section: En
December, 2014

Azerbaijan Journal of Physics

Fizika

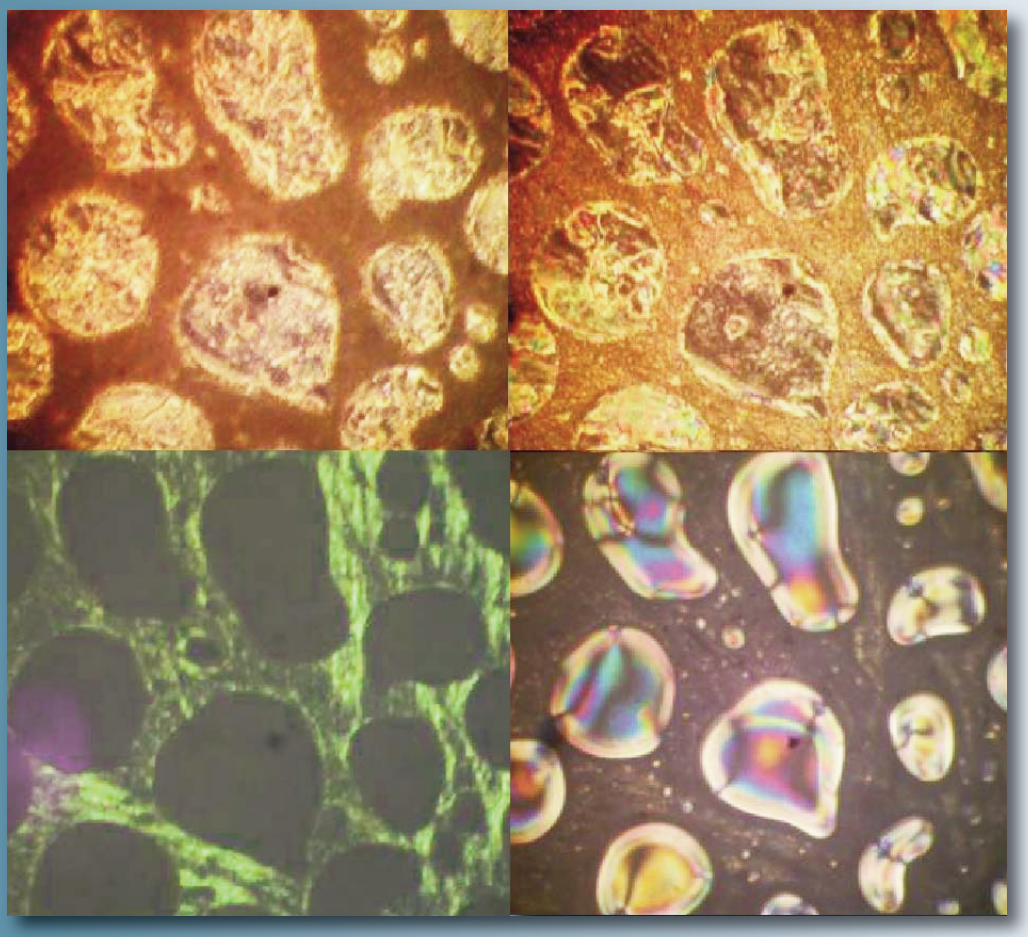

www.physics.gov.az

G.M. Abdullayev Institute of Physics
Azerbaijan National Academy of Sciences
Department of Physical, Mathematical and Technical Sciences

Published from 1995
Ministry of Press and Information
of Azerbaijan Republic,
Registration number 402, 16.04.1997

ISSN 1028-8546
vol. XX, Number 4, 2014
Series: En

Azerbaijan Journal of Physics

FIZIKA

G.M.Abdullayev Institute of Physics
Azerbaijan National Academy of Sciences
Department of Physical, Mathematical and Technical Sciences

PUBLISHING OFFICE

131 H.Javid ave, AZ-1143, Baku
ANAS, G.M.Abdullayev Institute of Physics

Tel.: (99412) 439-51-63, 439-32-23
Fax: (99412) 447-04-56
E-mail: jophphysics@gmail.com
Internet: www.physics.gov.az

It is authorized for printing:

Published at "**SƏRQ-QƏRB**"
17 Ashug Alessger str., Baku
Typographer : Aziz Gulaliyev

Sent for printing on: __.__. 201_
Printing approved on: __.__. 201_
Physical binding:_____
Number of copies:_____200
Order:_____

THERMODYNAMIC PROPERTIES OF Cu_5SmSe_4 RARE-EARTH SEMICONDUCTOR COMPOUND

Y.R. ALIYEVA, F.F. YAHYAYEV, T.R. MEHDIYEV
Institute of Physics of ANAS named by G.M. Abdullayev
AZ-1143, Baku, H. Javid ave., 33

Cu_5SmSe_4 is investigated by (DSC) differential scanning calorimetry method in temperature interval 100–600ºC. The compound thermodynamic parameters are calculated. The comparison of obtained DSC profiles at heating and cooling of Cu_5SmSe_4 shows the presence of thermal process hysteresis.

Keywords: differential scanning calorimetry, rare-earth semiconductor.
PACS: 65.40.Ba, 72.80.Ga

INTRODUCTION

The triple compounds of $A_5^{I}B^{III}C_4^{VI}$ type, in particular, Cu_5LnSe_4 with all elements introducing in Ln class are synthesized in [1-4]. Experimental investigations of Cu_2Se–Sm_2Se_3 system show the presence of five enough stable compounds $CuSmSe_2$, Cu_5SmSe_4, Cu_3SmSe_3, $CuSmSe_2$, $CuSm_5Se_8$. Cu_5SmSe_4 compound, thermodynamic parameters of which are given in ref. [8], forms with melting point 1333K at heating up to 1048K [3], The compound crystalline parameters published in [8] show on the fact that Cu_5SmSe_4 are crystallized in hexagonal structure with space group P3ml as other its analogues. The investigation results of Cu_5SmSe_4 compound by differential scanning calorimetry method which, as it is known, gives information on temperatures and phase transition heat (melting, crystallization, vitrification), thermodynamics and chemical reaction kinetics, chemical composition, purity, thermal and oxidative stability and etc. are given in present paper. On this method the heating is defined on heat flow, which is derivative of heating on time, that allows us to fix not only curves of heating (or cooling) of investigated sample but the presence of any phase transformation of first order.

EXPERIMENTAL PART

Cu_5SmSe_4 compound is synthesized in two stages. Cu, Sm and Se elementsof high purity in molecular ratio 5 : 1 : 4 are put in evacuated ampoule up to 1.3mPa on first stage. The ampoule is gradually heated, kept during 30 minutes at temperature 1353K. Further, the ampoule is cooled up to 1030K, kept during 170h. after that the temperature decreases up to room temperature. The experimental results of Cu_5SmSe_4 investigations carried out on XRD D8 ADVANCE (Brucker LTD, Germany) at temperatures 100, 150, 200, 300, 400, 700K are shown on fig.1.

The temperature dependences of “a” and “c” parameters and thermal expansion coefficient corresponding to them, are published in [5]. Differential scanning calorimetry (DSC) method is used with aim to study of peculiarities observed in temperature dependences of Cu_5SmSe_4 crystal lattice parameters. DSC experiments are carried out on installation NETZSCH DSC 204 F1 Phoenix 240-12-0141-L (Germany). The installation principle of operation is based on formation in calorimeter furnace of homogeneous temperature field in which the presence of phase transitions or reactions in sample leads to temperature gradient appearance.

The analysis of appearing gradients of thermal field and heat flows is carried out with the use of computer program Proteus. For investigation carrying out the samples of Cu_5SmSe_4 compound are previously grinded into powder, which is put in special crucible.

The crucibles of sample and etalon are put in calorimeter measured cell. The absence of zero line drift in scanning process provides the high accuracy and reliability of obtained experimental results.

The obtained results of DSC investigations of Cu_5SmSe_4 compound are shown on fig. 3-4. The scanning velocity in temperature interval from 100 up to 600ºC at heating and cooling of the sample is equal to 5ºC/min. The given velocity is totally satisfied to conditions guaranteeing the equilibrium of the thermal process carrying out from one side and the necessary relation of signal/noise which is enough for DSC profile registration. Al of mass 15mg and specific thermal capacity C_p=880J/kg·K is used in the capacity of etalon. The mass of investigated sample Cu_5SmSe_4 is equal to 100mg.

As it is followed from obtained experimental data (see fig.3), DSC scanning profile in heating mode has the two regions corresponding to endothermic processes in temperature intervals from 95 up to 155ºC and from 360 up to 482ºC, in which DSC minimums 141.5ºC (-0.06165mW/mg), 147.3ºC (-0.06221mW/mg), 397.0ºC (-0.0563mW/mg) and 469.8ºC (-0.09518mW/mg) are observed. The areas of these regions -3.925J/g, -0.6974J/g and -7.228J/g are proportional to reaction heats correspondingly.

Note that the form of these regions allows us to propose the presence of complex processes of phase transformations in them. From other side, it is necessary to note that temperature boundaries of these regions don’t achieve up to temperature 1048K at which Cu_5SmSe_4 compound formation takes place and moreover, its melting point 1333K. As it is followed from fig. 2, DSC scanning profile in cooling mode consists on the region corresponding exothermic reaction with maximum at temperature 456.9ºC (0.1608mW/mg) and region area 8.985J/g. The comparison of obtained DSC scanning

profiles at heating and then cooling of Cu_5SmSe_4 shows the hysteresis presence of thermal processes.

THE ANALYSIS OF EXPERIMENTAL DATA

As it is shown in [5], the temperature changes of«a» and «c» parameters of Cu_5SmSe_4 elementary cell have the nonlinear character showing on the fact that the increase of «a» and «c» parameters is observed in 100-400K interval, later, they decrease in temperature interval 400-550K and their increase is observed again at further temperature increase. The temperature change character of diffraction spectrum in interval 100-700K in [5] is estimated by three maximum positions: 2θ = 26.981; 30.88; 53.068 degree. It is well known that when linear expansion is linear function on temperature, then it is more obviously that it takes place along crystallographic axis. Such situation explains the obtained nonlinear temperature dependences for considered maximums of diffraction spectrum. Note that 2θ maximum interpretation is possible as result of several maximum impositions. In any case, the observable temperature changes of Cu_5SmSe_4 elementary cell parameters directly evidence on internal reconstruction of crystal structure. The explanation of temperature dependence of Cu_5SmSe_4 thermal expansion coefficient presents itself the enough complex task that according to phase diagram of Cu-Sm system in temperature interval from 860 up to 900ºC near Cu_5SmSe_4 temperature formation, it is possible the formation of Cu_6SmSe_4 and Cu_4SmSe_4 compounds. The similarity of diffraction spectra Cu_5SmSe_4, Cu_5Se_4 and Cu_7Se_4 allows us to propose that observable temperature changes are connected with phase transformations between compositions Cu with Se. The above mentioned is confirmed by coincidence of temperature regions on thermograms for parameter, for example "a" of Cu_5SmSe_4 elementary cell in which peculiarities are observed and also by phase diagram of analogous system Cu_2Se – Gd_2Se_3 [6] on which the possible phase transitions corresponding to Cu-Se system are well seen.

From above mentioned it is followed that phase diagram published in [3] doesn't totally reflect thermodynamic properties of Cu_2Se–Sm_2Se_3 system.

Note that the sulfur (selenium) forms the total cubic packing in which all tetrahedral voids taken by Cu^{1+} in well known structure of chalcosine cubic modification. Tetrahedrons have common edges (each edge belongs to two tetrahedrons) and totally fill the volume. Moreover, cuprum ions being in tetrahedrons form the clusters in which their interaction leads to $2Cu^{1+} \rightarrow Cu^{2+}$ substitution, i.e. $Cu_{2-x}S$ (Se) structure is defect one. Usually, $Cu_8{}^{+}Cu^{2+}S_5(Se_5)$ is one on each 10 tetrahedrons instead of $Cu_{10}S_5(Se_5)$ on the same volume. This chalcosine modification is stable at temperatures higher 420°C.

At temperatures below 420°C the structural transition in stable phase with closest hexagonal packing which is hexachalcosine is observed. The half part of Cu^{1+} ions posits in intervals of close-packed layer, i.e. they have the coordination number 3. The second half of ones posits in tetrahedron centers. The hexachalcosine structure is layered one, constructed from only triangles $CuS_3(Se_3)$ contacting by own sides that gives us the 16-electron configuration instead of normal one consisting of 18 electrons. By other hand, each Cu ion besides three sulfur ions, is surrounded on the same distances by three cuprum ions and therefore, electron deficiency is partly compensated because of metallic bond.

At temperatures less 103°C the monoclinic modification, which is called monocline chalcosine, becomes the stable one. Cu^{1+} ion with coordination number 3 shifts to triangle side and takes the coordination number (2+1). Cu^{+} ion being in tetrahedral coordination shifts to tetrahedron edge and has the coordination number 2.

Thus, parameter change peculiarities of Cu_5SmSe_4 elementary cell in temperature region from 100K up to 700K are well interpreted by phase transitions in cuprum polyhedrons. It is necessary to note that it is well known that polyhedrons with small coordination numbers which are excluded for rare-earth elements take part in phase construction of Ln-M-Z system (where Z are anions of VIb subgroup O, S, Se, Te; Ln are rare-earth elements; M are Cu^{1+}, Zn^{2+}, Cd^{2+}, Al^{3+}, Ga^{3+}, In^{3+}, Si^{4+}, Ge^{4+} and partly Ag^{1+}, Mg^{2+}, Fe^{2+}, Fe^{3+}).

All above mentioned is confirmed by published phase diagram of Cu-Se system and it is necessary to add that maximums on Cu_5SmSe_4 heating thermograms at temperatures: 52.59°C, 115.09°C, 147.59°C, 377.59°C and 470.09°C also agree with the given model, i.e. they are structural change results in cuprum polyhedrons [9]. The presence of narrow peak in heat capacity temperature dependence and also the observable temperature hysteresis allow us to confirm that in Cu_5SmSe_4 the phase transition of first order with temperature hysteresis ΔT~12.6° at 470.09°C temperatures is observed. Note that the temperature hysteresis is absent at the presence of narrow peak in heat capacity temperature dependence in phase transitions of second order [7]. Generally, the temperature hysteresis depends on temperature change velocity. The phase transition would take the place at temperature corresponding to equality condition of specific thermodynamic potentials under conditions of total thermodynamic equilibrium in system, which never realizes in experiment real conditions (even at infinitely slow temperature change). The point of phase transition of first order is characterized by Gibbs energy equality in phases between which the transition takes place: $\Phi_1(T,<p,<H) \equiv \Phi(T,p,H)$ though the derivatives of these thermodynamic potentials on parameters can't coincide. In the neighborhood of point of phase transition of first order the jumps of thermodynamic potentials are observed, the one of phases is absolutely stable one and another one is metastable one. As processes of thermodynamic equilibrium establishment don't slow down whereas the transformation process of one phase into another one slows down, then the temperature hysteresis is observed then the stable phase is firstly saved as metastable one in some parameter interval at passing of phase equilibrium point .

Taking into consideration the above mentioned, we have:

$$\left(\frac{\partial G}{\partial T}\right)_p = -S;\ \left(\frac{\partial G}{\partial p}\right)_T = V;\ \left[\frac{\partial\, G/T}{\partial\, 1/T}\right] = H$$

and therefore "jumps" should observe in point of phase transition on temperature dependences of entropy, enthalpy and specific volume. In Cu_5SmSe_4 case the above mentioned is demonstrated on fig. 3. The temperature maximums of DSC investigations of Cu_5SmSe_4 in heating and cooling modes are given in table 1. As the many experiments and analysis show, the amplitudes of four maximums: 52.59°C, 115.09°C, 147.59°C, 377.59°C in cooling mode are very small. The explanation of these results can be found in [9] generalized of many low-temperature phase investigations of Cu-Se systems for example [10-13]. The some results from [9] are represented in table 2 .

Table 1

	Maximum temperature, ºC				
heating	52.59	115.09	147.59	377.59	470.09
cooling					457.52
thermal hysteresis					12.57

Table 2

Reaction	Phase	Composition, at% Se	Temperature, °C from references		
			[11]	[15]	[16]
Peritectoid	$\beta Cu_{2-x}Se$, $\alpha Cu_{2-x}Se$, (Cu)	~33.3, ~33.3, ~0	123	131	138
Monotectic	$\beta Cu_{2-x}Se$, L_2, L_3	~36.5, ~52.5, …	523	523	523
Peritectic	$\beta Cu_{2-x}Se$, $\gamma Cu_{2-x}Se$, L_3	~36.5, ~50, …	377	382	384
Peritectic	$\gamma Cu_{2-x}Se$, $Cu_{2-x}Se$, L_3	50, 66.7, …	332	342	343
Euitectic/ Peritectic	$Cu_{2-x}Se$, (Se), L_3	66.7, ~100, …	218	218	226
Euitectic/ Peritectoid	$\gamma Cu_{2-x}Se$, $\beta Cu_{2-x}Se$, $CuSe_2$	~50, ~50, 66.7	~120	…	…
Euitectic/ Peritectoid	$\gamma Cu_{2-x}Se$, $\beta CuSe$, $\beta Cu_{2-x}Se$	~50, ~50, ~36.5	~120	…	…
Peritectoid	$\beta Cu_{2-x}Se$, Cu_3Se_2, $\beta CuSe$	~36.5, 40, 50	112	135	143
Euitectoid/ Peritectoid	$\beta Cu_{2-x}Se$, $\alpha CuSe$, $CuSe_2$	~50, ~50, 66.7	~51	53	60
Euitectoid/ Peritectoid	$\beta Cu_{2-x}Se$, $\alpha CuSe$, Cu_3Se_2	~50, ~50, 40	~51	…	…

Note that Cu_2Se compound in considered temperature interval takes part in seven reactions enduring the different transformations and forming $Cu_{2-x}Se$ phase with Se excess. The homogeneity region of $Cu_{2-x}Se$ at room temperature corresponds to Se change in limits from 33.3 and 36.0 at.% (table 2) that corresponds to "x" change in interval from 0.18 up to 0.22. $Cu_{2-x}Se$ homogeneity region width increases with temperature increase taking the region from 75°C up to 500°C [9, 10-15].

In [9,10,11] it is mentioned that less 123°C at polymorphous transformation $\alpha \leftrightarrow \beta$ in αCu_2Se phase the reaction goes very slowly. The reaction slow behavior doesn't allow us to obtain αCu_2Se pure phase at even very slow scanning. In [13] it is shown that existence region width is very small. By other hand, Cu_3Se_2 (umangite) phase appearing in peritectic reaction between βCu_2Se and $\beta CuSe$ less 135°C is also going very slowly [14]. Note that at temperature near 120°C it is possible the observation of low- and high-temperature phases of Cu_5Se_4 composition [16].

In temperature region higher 300ºC as a result of peritectic reactions ($\beta Cu_{2-x}Se$ and Se) and ($\gamma Cu_{2-x}Se$ and Se) CuSe and $CuSe_2$ phases form but as it is shown in [9], CuSe formation reactions go slowly than inverse ones. In [17] it is shown that at temperature near 80ºC Cu_7Se_4 metastable phase forms, which recrystallizes in CuSe at temperature 170ºC in the presence of amorphous selenium. Moreover, at temperature 160ºC the partial selenium enrichment CuSe into $CuSe_2$ is observed which later is finally dissociated into CuSe at 210ºC.

Using the above mentioned data the following interpretation of Cu_5SmSe_4 obtained results becomes obvious one. The maximums observed at temperatures 470.9ºC (heating) and 457.52ºC (cooling) are interpreted as phase transitions $\beta \rightarrow \gamma$ (heating) and $\gamma \rightarrow \beta$ (cooling) into Cu_2Se (from hexagonal modification into cubic one). The maximum at temperature 147.59ºC is interpreted as phase transition $\alpha \rightarrow \beta$ of Cu_2Se (from rhombic modification into hexagonal one).

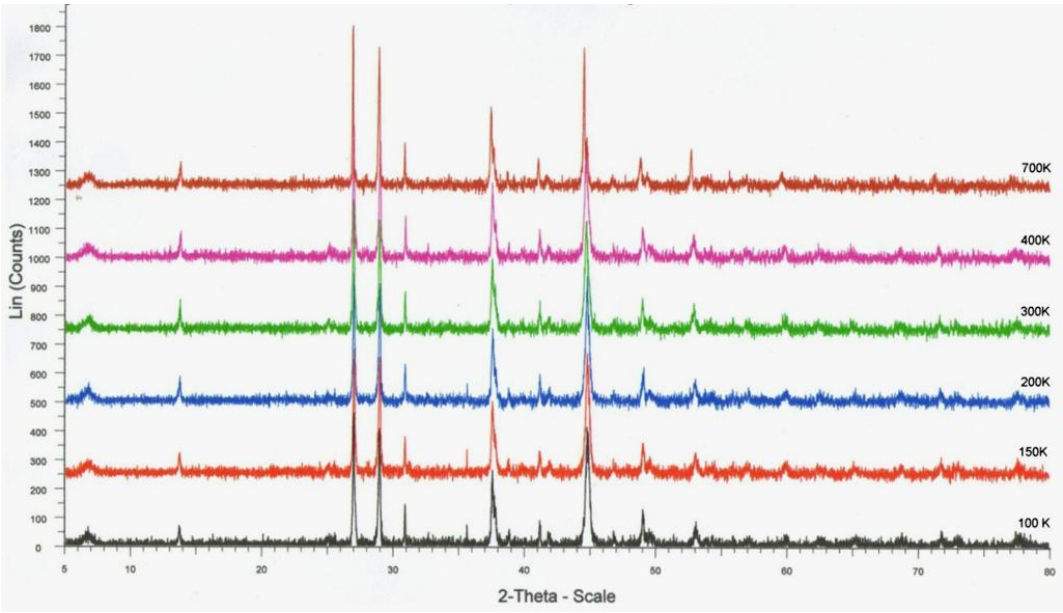

Fig.1. Powdergrams Cu_5SmSe_4 obtained at temperatures 100, 150, 200, 300, 400, 700K.

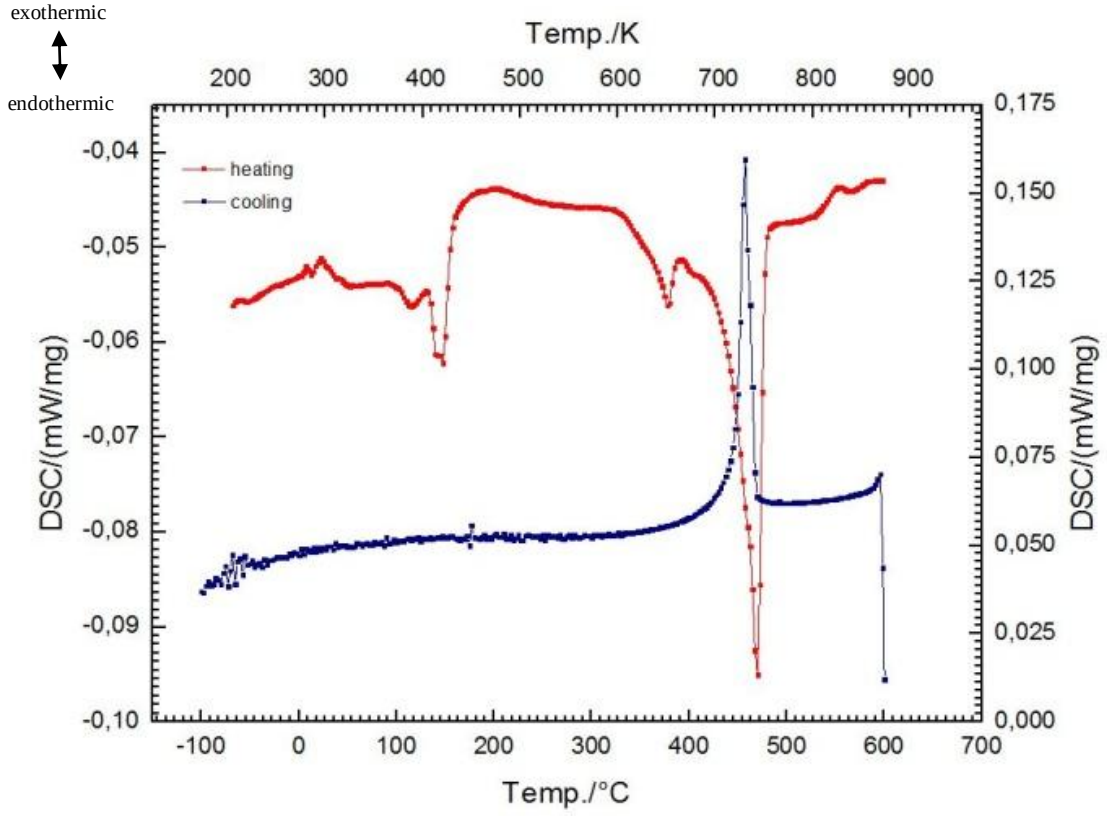

Fig.2. DSC scanning profiles Cu_5SmSe_4: red one is heating, blew one is cooling.

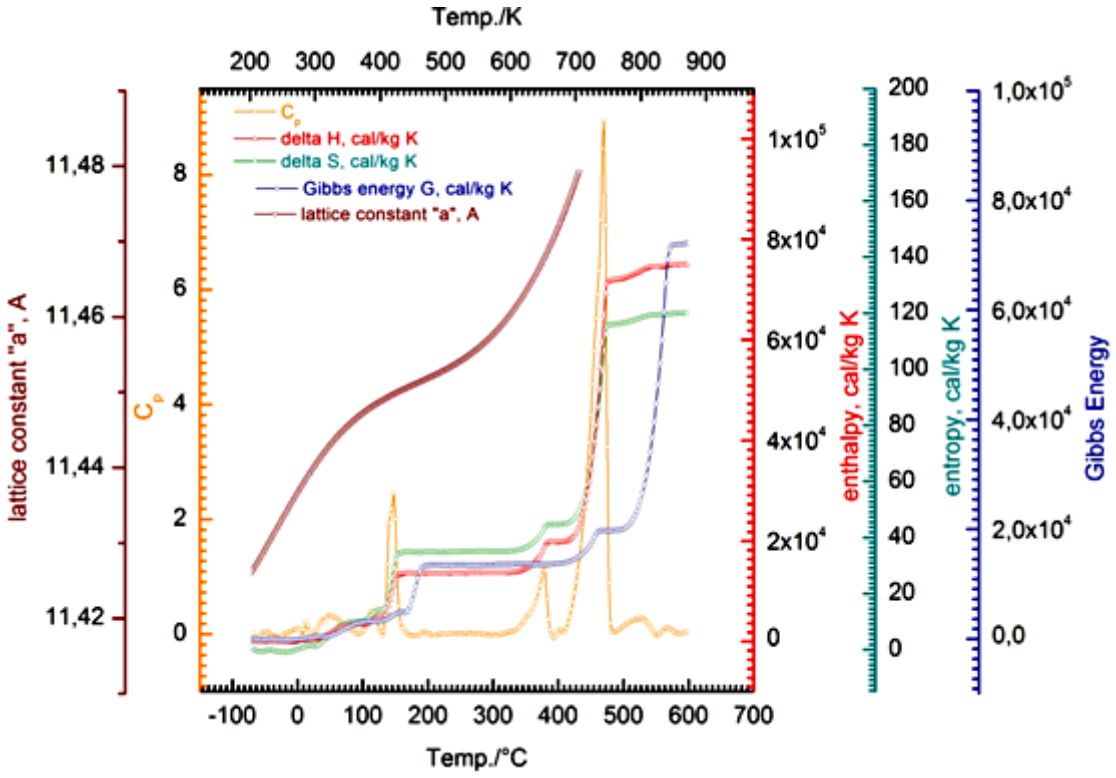

a)

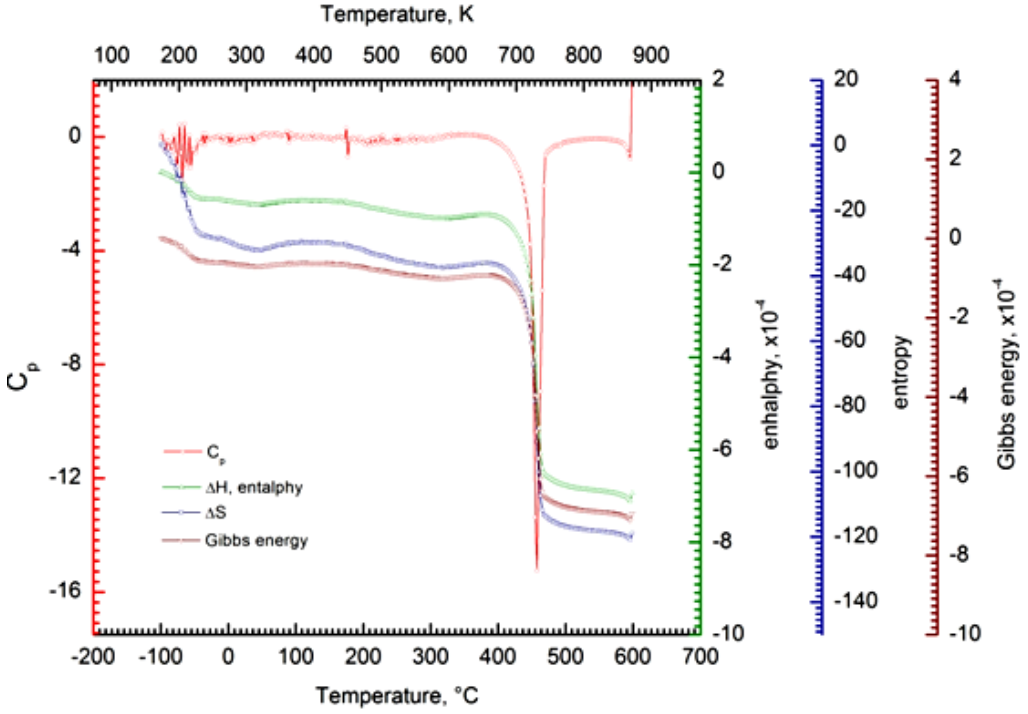

b)

Fig.3. a) Cu_5SmSe_4 thermograms obtained in heating and cooling modes. *b)* The heat capacity, enthalpy, entropy and Gibbs energy are given. The "a" parameter temperature dependence of Cu_5SmSe_4 crystal lattice is given for comparison on heating thermogram.

[1] *P.Q. Rustamov, O.M. Aliev, Q.Q. Quseynov i dr.* Neorqan. materiali. 1976. t. 12. № 7. s. 1192–1195. (in Russian).

[2] *P.G. Rustamov, O.M. Aliev, T.Kh. Gurbanov.* Troynie khalkoqenidi redkozemelnikh elementov. Baku: Elm, 1981. 228 s. (in Russian).

[3] *N.Yu. Pribilskiy, R.S. Hamidov.* JNX. 1983. t. 28. № 2. c. 719–723. (in Russian)

[4] *E.P. Alieva, I.Ya, Aliev, Z.Ya. Suleymanov, A.S. Abbasov.* Fizika. 2007. t. 13. № 4. s. 134–135. (in Russian).

[5] *R.N. Ragimov, E.P. Alieva, A.S. Amirov, G.G. Guseynov.* ANAN "Izvestiya" F.M.T., fizika i astronomiya, 2012, tom XXXII , № 2, s. 60-65. (in Russian).

[6] *P.G. Rustamov, O.M. Aliev, A.B. Eynullaev, I.P. Aliev. Kh*imiya redkikh elementov. Khalkolantanati redkikh elementov. Moskva «Nauka – 1989», s. 206. (in Russian).

[7] *Yu.M. Gufan.* Sorosovskiy obrazovatelniy jurnal, Rostovskiy gosudarstvenniy universitet, Rostovskiy gosudarstvenniy universitet, Rostov-na-Donu, №7, 1997, 109-115. (in Russian).

[8] *E.R. Alieva, I.Ya. Aliev, Z.I. Suleymanov, A.S. Abbasov.* «Fizika», tom XIII, № 4, Baku, «Elm», 2007 , str. 134-135. (in Russian)

[9] *D.J. Chakraborti and D.E. Laughlin.* The Cu-Se (Copper-Selenium) System, Bulletin of Allow Phase Diagrams, v.2, No 3, 1981, p. 305-315.

[10] *R.M. Murray and R.D. Heydmg.* C.a11. J. Chem., 53(6),p 878-887 (1975).

[11] *A.L.N. Stevels and J. Jellinek.* Rec. Trav Chim., 90.p 273-283 {1971).

[12] *Z. Ogorelec, B. Mestnik, D. Devcic.* J. Mater. Sci., 7(8).p 967-969 (1972).

[13] *A.L.N. Stevels.* Philips Res. Rep. Suppl. No.9, p.1-124, 1969.

[14] *R.D. Heyding.* Can. J. Chem., 44(10), p.1233-1236, 1966.

[15] *G.P. Bernardini and A. Catani.* Miner. Deposita (Berl.), 41(3), p.565-586, 1972.

[16] *D. C. Harris, L. J. Cabri and S. Kaiman.* Athabascaite; a new copper selenide mineral from Martin lake, Saskatchewan, Can. Mineral, April 1970, v. 10, p. 207-215.

[17] *Woo Kyoung Kim.* Study of reaction pathways and kinetics in $Cu(In_xGa_{1-x})Se_2$ thin film growth, PhD Dissertation, University of Florida, 2006, 237p.

Received: 22.10.2014

THE FEATURES OF ELECTROCHEMICALLY DEPOSITED CdS THIN FILMS

Sh.O. EMINOV, E.K. HUSEYNOV, Kh.D. JALILOVA, N.J. ISMAILOV, A.A. RAJABLI , G.Kh. MAMEDOVA, J.A. GULIYEV
Institute of Physics of NAS Azerbaijan, Baku
e-mail shikhamirem@gmail.com

The stoichiometric CdS films were successfully deposited on ITO glass substrate using electrodeposition techinuque from non-aqueous solution of 0.055M $CdCl_2$ and 0.19M elemental sulfur, dissolved in 50 mL dimethyl sulfoxide (DMSO) at 110-120°C. The films were characterized for optical properties and EDX composition. The SEM images shows uniform thin film CdS. EDX analyze shows that the composition of Cd and S may considered to be stoichiometric. The optical band gap of as grown CdS is measured to be 2.42 eV.

Keywords: Solar cells, CdS, thin films , optical transmission , electrodeposition.
PACS: 81.05.RM,81.16Pr; 81.07.Pr ; 68.43.Hn.

INTRUDUCTION

The dramatic climate change, the limited reserves of fossil fuels and energy security concerns have spurred internationally unprecedented interest in developing renewable energy technologies from sustainable and renewable energy resources. Solar energy represents one of the most abundant and yet least harvested sources of renewable energy. A solar cell (also called a photovoltaic cell) is an electrical device that converts the energy of light directly into direct current electricity (dc) using semiconductors that exhibit the photovoltaic effect. Electrons in a solar cell absorb photon energy in sunlight, which excites them to the conduction band from the valence band. This generates hole-electron pairs, which are being separated by a potential barrier (such as a *p-n* junction) and induces a current, as shown in fig.1, where heterojunction band diagram of a CdTe/CdS photovoltaic system was illustrated.

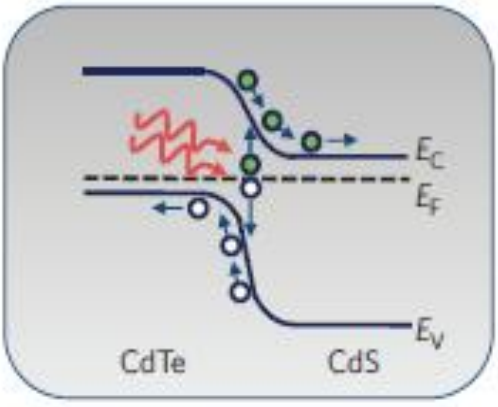

Fig. 1. Heterojunction band diagram CdTe/CdS PV-cell.

Because intermittent nature of solar energy, efficient energy storage systems are critically needed to make the optimal of the electricity generated from these sun cells since they can promote the reliability and effective use of the entire power system by storing energy when in excess while releasing it when in high demand. Thus the energy of the photovoltaic cells can either be used directly or be used to recharge storage devices (batteries and capacitors) which in turn can power the application electronics when the Sun is not shining. As shown in Fig. 2, typical photovoltaic solar energy harvesting system includes PV cells which are often electrically connected and encapsulated as module (1), inverter (2) to convert dc electricity produce by PV-cell to ac electricity as well as energy storage systems (3), such as batteries or electrochemical capacitors (ECs). A variety of materials and processes can potentially satisfy the requirements for PV energy conversion, but in practice nearly all photovoltaic energy conversion uses semiconductor materials in the form of p-n- and hetero-junctions.[1-3]. Conventional solar cells are constructed from junctions of p- and n-type semiconductors, where the electrostatic potential at the interface provides the driving force for charge separation. Most of the currently available commercial devices based on the uses of silicon *p-n* junction. Crystalline Si has continued to lead the market in the worldwide adoption of solar energy with over 85% market share [1]. Modern commercial Si mono-crystalline solar cells produce about 22.5% conversion efficiency According to various researchers it is not theoretically possible to convert more than 29% percent of the light into energy using crystalline solar cells. Realistically, the limit for a PV panel is likely closer to 24 to 25%. The losses due largely to practical concerns like reflection off the front surface and light blockage from the thin wires on its surface. Though highly efficient cells have been fabricated in the laboratory, practical application of such devices is limited due to the cost of producing and refining such pure material and the associated device fabrication.

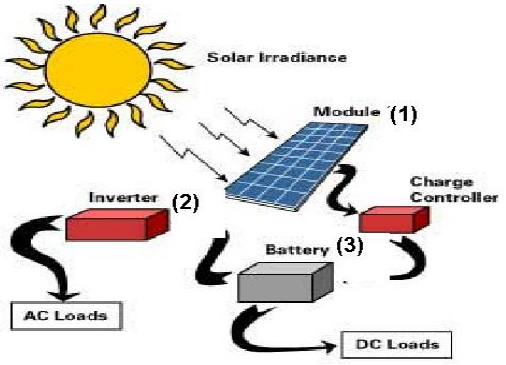

Fig. 2. The scheme of sun harvesting system.

Second generation solar cells are based on heterojunctions of thin layers of different semiconductor materials. Among all types of solar cells, cadmium sulfide (CdS) - cadmium telluride (CdTe) and cadmium sulfide (CdS) - copper indium diselenide ($CuInSe_2$ or CIS) heterojunctions based thin film solar cells are of great interest due to their high efficiency and low cost [1] [4-7]. In these cells CdS is commonly used as a window layer, while CdTe was found to be a very suitable absorbing layer for solar cells due to its direct band gap of ~1.5 eV close to the optimum band gap for PVs.

The CdS/CdTe based solar cells have reached an efficiency of 16.5% which is close to the predicted efficiency limit of 17.5%. This kind of solar cells has been used for a long time and still being widely used nowadays. However, due to a lot issues associated with the fabrication procedures of CdTe-CdS solar cells (including ohmic contact problems) they are not much more efficient than silicon solar cells as we might expect. CIS is another promising absorber material among all thin film absorbers. High performance CdS/CIS based solar cells with an efficiency of 19.5% have been reported on the laboratory scale and 10.3% over large surface of 3860 cm^2. Molybdenum is usually used as the contact material for CIS because it forms non-rectifying ohmic contact with CIS. So far the most efficient CIS based solar cells are almost all made by vacuum co-evaporation of the three elements (Cu,In, Se) and they generally apply a structure of glass/Mo/CIS/CdS/ITO which is called the front wall structure . A reverse structure which is so named back wall structure of glass/ITO/CdS/CIS/Mo is also adopted by some research groups. With the back wall structure, people have achieved an efficiency of 5.0% by spray technology and 8.1% by co-evaporation. Further improvement in power conversion efficiency over the traditional PV device structure can be achieved by tuning the optical and electric properties of the light absorption layer as well as the window layer, utilizing nano-template-assisted patterning and fabrication.

n-CdS is an II-VI wide direct band gap (2.42 eV) semiconductor. This particular property makes it a key element for solar cell applications and is a commonly used n-type semiconductor as a window layer for heterojunction solar cell application. Additionally, CdS thin film has a broad range of another application in important technical fields such light emitting diodes large screen liquid crystal devices, gas sensors and field effect transistors.

In last decades, efforts have been devoted to the preparation of high quality CdS thin films and nanostructures and its investigation. Many techniques for deposition of CdS thin films were reported, such as sputtering, chemical bath deposition, metal vapor oxide deposition (MOCVD), sputtering, spray deposition and electro-deposition method [8-12].

In this work we report synthesis of CdS thin films electrochemically deposited over conducting ITO-glass substrates and its characterization by various techniques like XRD, SEM, and optical transmission spectroscopy**.** We have chosen electrochemical deposition route to deposition because it offers deposition over a large area, as well as due to other advantages such as a low temperature operation, flexible process control and economic [10].

EXPERIMENTAL DETAILS

Deposition. The electrochemical deposition was carried out in 150 mL two-electrode cell unit equipped with heater, thermo controller and stirrer. Commercial glass slides covered with a transparent and conductive tin-doped indium oxide (ITO) film sputtered by magnetron deposition are used as working electrode.

The electrolyte for CdS deposition was composed of non-aqueous solution of 0.055M $CdCl_2$ and 0.19M elemental sulfur, dissolved in 50 mL dimethyl sulfoxide (DMSO) at 110-120°C. Sulfur was dissolved in the solution at 150°C during 1 hour.

Electroplating tape (3M) was placed across the width of the ITO coated side of the sample where it crossed the solution/air interface when the sample was placed in solution. This was done because we had previously observed this region to be electrochemically very active during voltage application causing a thin section of ITO at this interface to erode across the entire width of the sample, breaking the electrical contact to the rest of the film. Covering this interface area eliminated the problem.

Glass-ITO substrate was mounted vertically inside of the cell containing the solution. Under dc electrodeposition condition, a constant current density of 15mA/cm^2 was applied for 10-100 sec. After the deposition was complete, the substrate were removed from the cell and were allowed to dry in air. The dried samples were rinsed with acetone with aim to remove the excess of Sulfur from the surface and finally dried. The samples were then dipped in saturated $CdCl_2$ in methanol solution and annealed in air at 400°C for 10 minutes. The aim of this step was to facilitate the recrystallization and purification of CdS films and condition the surface prior to CdTe deposition.

Characterisation: The surface microstructure were observed using scanning electron microscope (SEM) JEOL model JSM 5600 LV, Energy Dispersion X-ray analysis (EDX) Germany) was also done (using Bruker Nano GmbH, Berlin), to confirm the presence of possible elements in the deposited film. Optical analysis of CdS film samples with different thickness deposited over glass during different deposition duration was performed using optical transmittance spectra in room temperature and at a region from 1.0 to 4.0 eV; SEM and EDX characterizations were conducted at the Institute for Research and Development of Photovoltaic Energy, Paris, France (IRDEP), while the Optical analysis was performed in Institute of Physics of Azerbaijan NAS.

RESULTS AND DISCUSSION

Thickness of as grown films varried from 6 nm to 1.5 mkm depending on deposition time. The optical photograph of the film is shown on Fig. 1, while SEM images of CdS films fabricated on the glass/ITO substrate are shown on Fig. 2. As it can seen from the photographs, is the CdS film has fine grains with diameter about of 1.5-2 μm. Thick films has net of deep cracks,

which are induced by mechanical stress on the interface with substrate .

EDX spectrum is shown on Fig. 3, while the the detailed spectrum data is presented in the Table 1. In figure 3 it's very evident that there are 6 peaks in the spectrum, which are originated from Cd, S, O,Si, Cl and In. By comparing with intensity on Cd peak (39 at. %,) and S (37.22 at.) % we could identify the composition of Cd and S to approximately 1:1and may considered to be stoichiometric . Apparently, the occurrence of Cl (4.86% at.) is because $CdCl_2$ was used as component of the electrolyte solution. The occurrence of Si peak(0.3at.%) is because of deposition was conducted on glass substrate, while the occurrence of In peak (0.1 at. %) is because the sample was coated with ITO to facilitate electrical conduction. The spectrum is revealed occurrence of high level of Oxygene wt% is reached to 18-20% .

Table 1. EDX Spectrum data.

Elements	**Series**	**wt.%]**	**[at.%]**
Cadmium	L-series	72.38	39.14
Carbon	K-series	0.00	0.00
Oxygen	K-series	4.84	18.39
Silicium	K-series	0.14	0.30
Sulphur	K-series	19.63	37.22
Chlor	K-series	2.83	4.86
Indium	L-series	0.17	0.09
Total:		100.00	100.00

The formation process of CdS induced by continuously electrochemical reduction of $S_2O_3^{2-}$ was expressed as follows [13] :

$$S_2O_3^{2-} + 6H^+ + 4e^- \rightarrow 2S + 3H_2O$$

$$S + H^+ + 2e^- \rightarrow HS^-$$

$$Cd^{2+} + HS^- \rightarrow CdS + H^+$$

The UV-visible spectrums of glass/ITO substrate and thin films of CdS with different thicknesses: 6 nm, growth time t=20 sec.; 2- 30 nm, t=50 sec; 3 - 43 nm, t=80 sec, consequently. We have determined band gap of our samples by Tauc's formula to be as 2.42 eV which coincided with dates reported earlier.

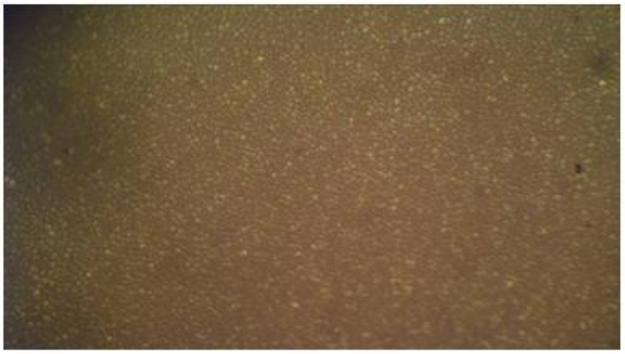

Fig.3. Optical photograph of as grown CdS film.

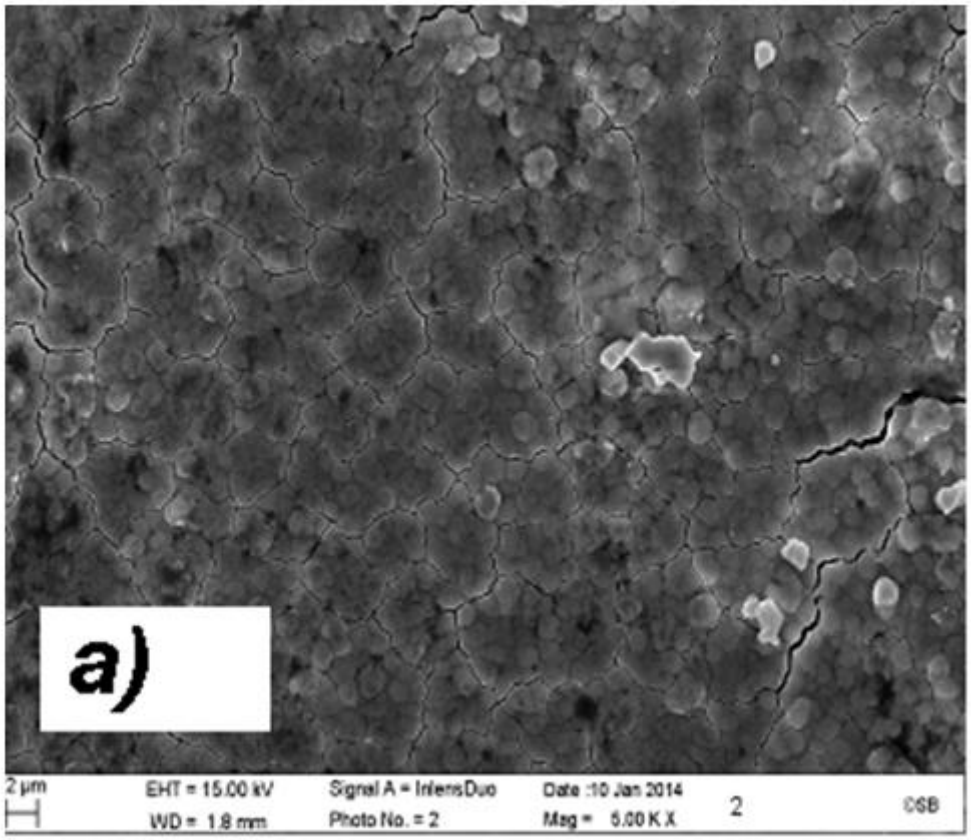

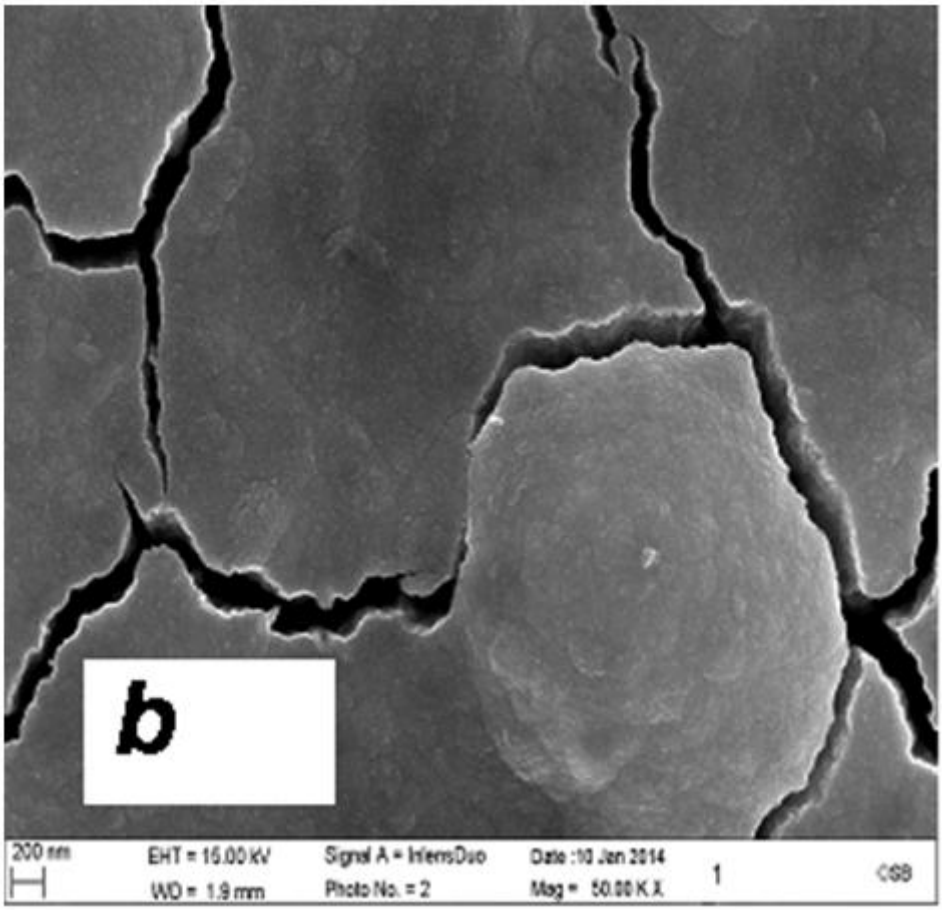

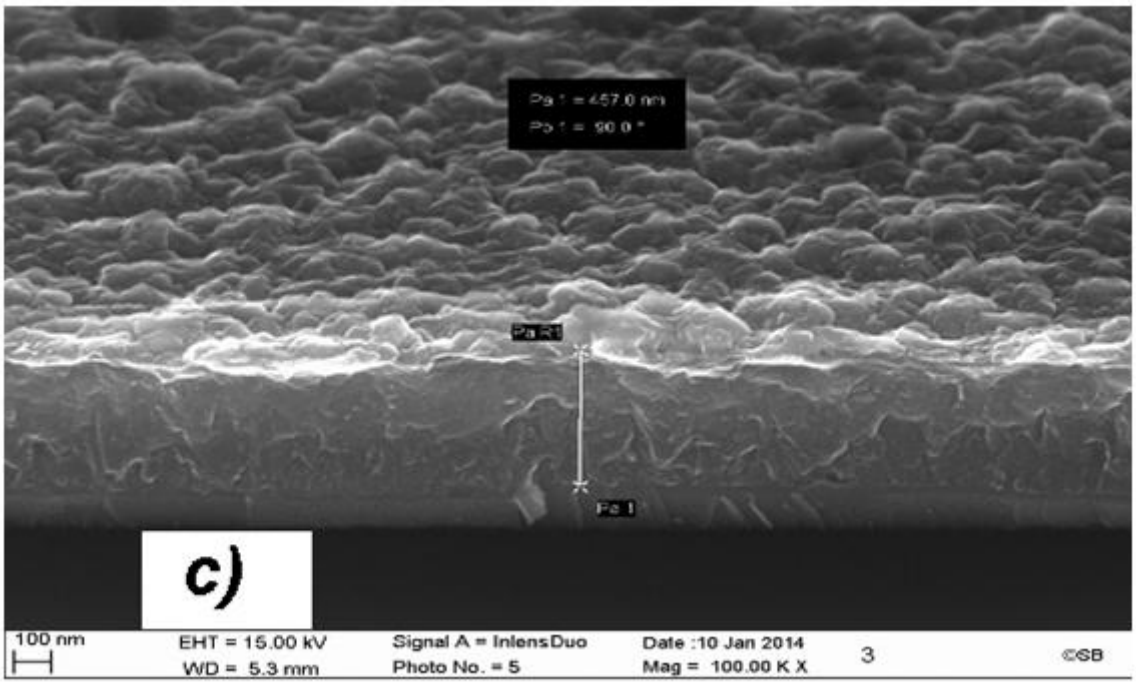

Fig.4. SEM images of a CdS thin film: a) multiplication X 5x 10^3;b) x 10^5; c) cross-section image of a film with thickness of 450 nm.

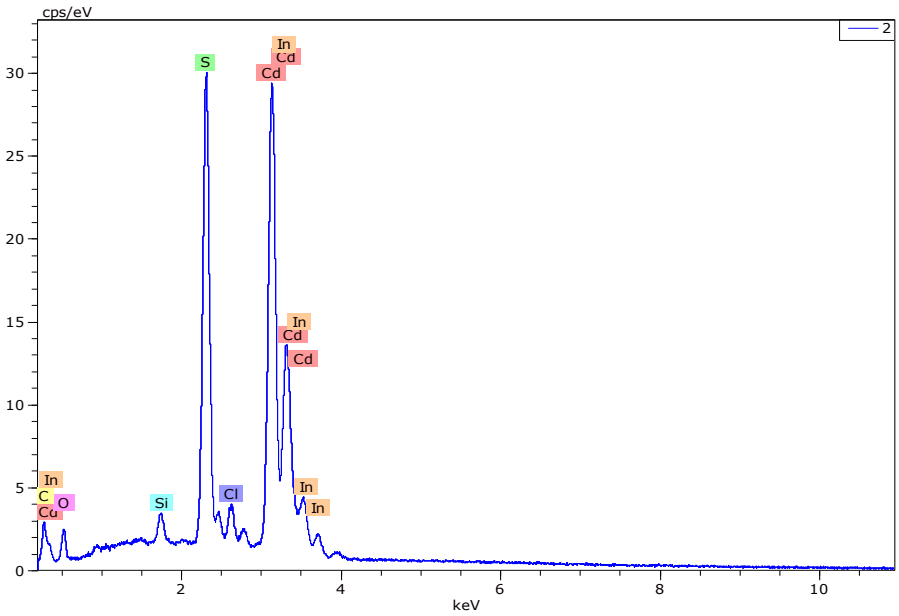

Fig.5. EDX spectra for CdS deposited on the glass/ITO substrate.

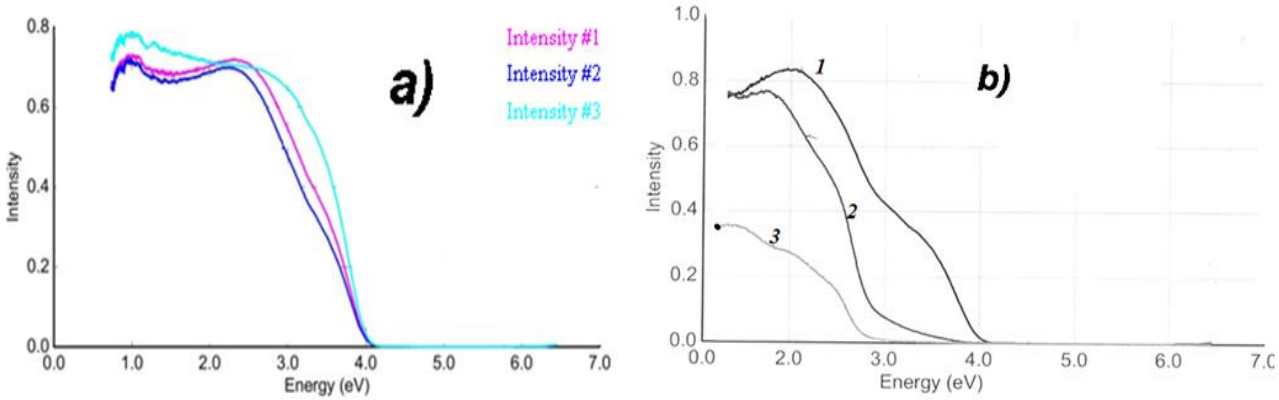

Fig. 6. a) UV-Visible spectra for glass/ITO substrate; b) UV-Visible absorption spectra for CdS films with different thickness deposited on the glass/ITO substrate.

CONCLUSION

The stoichiometric CdS films were successfully deposited on ITO glass substrate using electrodeposition techinuque from non-aqueous solution of 0.055M $CdCl_2$ and 0.19M elemental sulfur, dissolved in 50 mL dimethyl sulfoxide (DMSO) at 110-120°C. The films were characterize and for morphological and optical properties as well as EDX composition. The SEM images shows uniform thin film CdS. EDX analyze shows that the composition of Cd and S is approximately 1:1and may considered to be stoichiometric .The optical band gap is measured to be 2.42 eV.

ACKNOWLEDGEMENTS

The authors is grateful to Prof. Daniel Lincot and Serena Gallanti (IRDEP, France) for providing date of SEM and EDX measurements.

[1] *T.S. Ravi.* Technology development for high-efficiency solar cells and modules using thin (<80 µm) single-crystal silicon wafers produced by epitaxy, Subcontract Report NREL/SR-5200-58593 May 2013.

[2] *Liu Piao.* Heterojunctions and Schottky diodes on semiconductor nanowires for solar cells *Doctoral Dissertations* (2010). http://uknowledge.uky.edu/gradschool_diss/77

[3] *A.H. Hochbaum, P. Yang* Semiconductor nanowires for energy conversion ,Chem. Rev.,2010, 527-546.

[4] *P. Jackson, et al*. Prog. Photovolt Res.Appl. , 2011, 19, 894- 897.

[5] *A. Romeo, M. Terheggen* Prog. Photovolt: Res. Appl. 2004; 12:93–111.

[6] *A. Chirilă, P. Reinhard et al.* Nature Materials, 2013, 12, 1107–1111.

[7] *P. Reinhard, et al*. IEEE J. Photovolt. 2013, 3,, 572–580.
[8] *Ryo Asaba, Kazuki Wakita,Atsushi Kitano, Yong Gu Shim, Nazim Mamedov, Ayaz Bayramov, Emil Huseynov, Ilham Hasanov.* Physica Status Solidi,C10,7-8, 2013, 1098-1101.
[9] *S.Rajpal, V.Bandyopadhyay*. Journal of Nano and Electronic Phys. 2013, 5, 03021.
[10] *A.,Hasnat, J. Podder*. J. Bangladesh Academy of Science, 37, 1, 2013, 33-41.
[11] *N.P. Klochko* Functional Materials, 2007, 14, 2 195-199.
[12] *M.N. Mammadov, A.Sh. Aliyev, M. Elrouby* Int.J. Thin Film Sci. Tec. 1, 2, 2012, 43-53.
[13] *Lu C. Wang X.,Xu J. et al*. Electrochem. Commun, 2008, 10. 3749-3755.

Recevied: 16.09.2014

THEORETICAL CALCULATION OF SPATIAL AND ELECTRONIC STRUCTURES OF THE COMPLEX OF OLIGOMER OF POLYETHYLENE GLYCOL PEG4 WITH NaCl ION PAIR

S.D. DEMUKHAMEDOVA, Z.I. HAJIYEV, I.N. ALIYEVA, N.M. GODJAEV
Institute for Physical Problems, Baku State University, Azerbaijan
AZ-1145, Baku, Z.Khalilov str., 23
svetlanabest@mail.ru

In this paper the spatial and electronic structure of the organic polymer which is polyethylene glycol (PEG4) oligomer complex with NaCl ion pair was calculated on base quantum chemical ab initio Hartree-Fock method using the 6-31G basis. The study model is obtained by preliminary simulation based on molecular dynamics simulations. The calculation of the energy and geometrical parameters of the complex, the analysis of the main structural changes and changes in the electronic structure at formation of the complex of polyethylene glycol oligomer with NaCl ion pair were carried out. A comparison of the resulting complex with the previously studied complexes of oligomer PEG4 with sodium atom and a chlorine atom was carried out. The calculations confirmed that the stabilization of these complexes is provided due the sodium cation interactions with the oxygen atoms and the anion chlorine interaction with the hydrogen-terminated polyethylene glycol chain.

Keywords: oligomers, polyethylene glycol, complex, quantum-chemical calculations, structure, the molecular orbitals
PACS: 31.15.-p; 31.15.E

INTRODUCTION

Nowadays the methods of molecular modeling and calculating quantum chemistry are irreplaceable instrument in structure investigation and polyatomic molecules allowing us to solve the wide spectrum of tasks, which are unsearchable for experimental investigation methods. In particular, they are used for investigation of structural-functional bonds in biomolecules, investigations of separate molecule properties and their complexes and for searching of new medicines. The controllable polymer structure formation by the means of ordered arrangement of other material in it, are one of more perspective directions at obtaining and perfection of new materials with earlier given properties. Last time the developments of different systems of medicine delivery directly in cell by the way of intracellular transport are actual ones.

The polymer complexes with metal cations or anions, which have the wide spectrum of possibilities at variation of physicochemical complex properties, have the essential meaning. The development of new DNA delivery systems with use of cationic polymers for gene delivery in cancerous cells with the help of genic therapy is carried out. As a result of experimental investigations [1] it is proved that such polymer complexes with ligand in difference on non-ligand ones, begin to accumulate in cells that allows us to increase the medicine delivery efficiency directly to ill cells [1].

Polyethylene glycol is enough often chosen in the capacity of polymer because of its ability to space self-organization round the charged groups. In particular, the polyethylene glycol ability (PEG) to form the stable complexes with alkali metal ions having the big practical use [2,3] is well known.

The [4-13] are dedicated to mass-spectroscopic investigation methods of polyether complexes structure with alkali metal ions and modeling of their interactions by molecular mechanic methods. It is shown that polyether chains are bended round the alkali metal ions forming the structure in which oxygen atoms turn round to ion and, also, the chelatation of ion by double- end OH-groups is possible.

PEG4 and PEG5 polyethylene glycol oligomer complex spatial structures with atoms of sodium, potassium and chlorine are earlier investigated by quantum chemistry methods [15-21]. The theoretic modeling and quanto-chemical calculation of oligomer complex with organic polymer PEG4 with NaCl ion pare are given in present paper.

CALCULATION METHODS

The molecular dynamic method from ChemOffice programs package for molecular modeling is used on the first stage of calculation for formation of PEG+Na complex. This method using the force field of atom-atom potential allows us to study the complex conformation mobility observing the detail microscopic picture of inner thermal mobility of forming complex in sub-nanosecond time intervals. The quantum-chemical calculations of complex obtained structure are carried out within framework of *ab* initio Hartree-Fock method approximation with use of GAUSSIAN-09 program complex. Non-empiric Hartree-Fock method isn't required knowledge of any empiric parameters for calculation carrying out as distinct from molecular-mechanical and semi-empirical methods and at correct usage the non-empiric methods give the big reliability of chemical compound property estimation. The choice possibility of different atom orbitals (AO) (basis sets) is provided in them. AO flexibility increase is achieved by use of valence-disintegrated basis sets. The basis 6-31G, the frame orbitals in which consist of six Gaussian functions and valence orbitals divide on two components: compact component consisting of three Gaussian functions and diffusion one which is presented by one Gaussian function, has the most dissemination The valence orbital compression [14] is taken into consideration in valence- disintegrated basis 6-31G. The

errors of measurement of bond lengths and valence angles are ~1%, electric density is defined with accuracy ~10%, conformation transition energy (rotation and inversion barriers) is defined with error $\leq$ 2kcal/mol. For carrying out of calculations firstly the developed model of polyethylene oligomer consisting of four PEG4 repeated links, to the middle of which NaCl ion pare is displaced on distance of Van-der-Waals contacts, is modeled. The structure obtained because of optimization by method of molecular dynamics is stabilized due to oxygen atom contacts of polyethylene chains with sodium cations and, also, hydrogen atoms with chlorine anions of NaCl ion pare. The geometric, energy and electron parameters of PEG4+NaCl complex are obtained on the base of following quantum-chemical calculations carried out within framework of Hartree-Fock theory (HF) by Gaussian-09 program with 6-31G (p,d) basis use. Taking under consideration the fact, that we are going to study the vibrational absorption spectrum of polyethylene glycol complex with NaCl ion pare the calculation of spatial and electron structure of PEG4+NaCl complex by DFT/B3LYP method in the same basis 6-31G (p,d) in the used Gaussian-09 program package is carried out. It is known, that the method of density functional theory DFT with hybrid functional B3LYP is better optimized one for calculation of vibrational spectrum frequencies.

RESULTS AND THEIR DISCUSSION

The organic polyethylene glycol polymer PEG4 structures with NaCl ion pare, obtained as a result of theoretical modeling, are given on fig.1 (a-d).

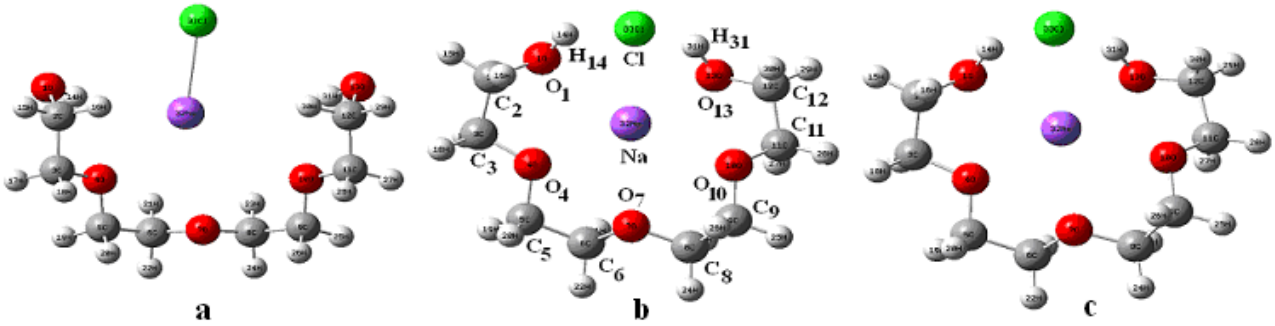

Fig. 1. Space structures of polyethyleneglycol complex models PEG4+NaCl: (a) after molecular dynamics; (b) after optimization by ab initio HF method; (c) after DFT/B3LYP optimization by method

As it is seen from Fig.1, the structure obtained after optimization by B3LYP method practically doesn't differ on structure obtained after optimization by HF method. The only elaboration of some structural parameters is carried out in this calculation process.

The spatial structure calculation results, in particular, the optimized values of geometric parameters: bond lengths, valence and double-edge angles in PEG4 complex with NaCl ion pare and also for comparison the corresponding values of pure PEG4 structures of earlier studied by us and its complexes with atoms of sodium and chlorine [15-18], are given in tables 1-3.

As it is seen from table 1, according to calculation results by B3LYP method the insignificant increase of bond length is observed in average on 0.02 Å.

Table 1.

Bond lengths (Å) in optimized complexes of PEG4 polyethylene glycol with atoms of sodium, chlorine and NaCl ion pare

Bond	PEG4 and its complexes				
	PEG4 (HF)	PEG4+Na (HF)	PEG 4+Cl (HF)	PEG 4+NaCl (HF)	PEG 4+NaCl (B3LYP)
O1-C2	1.40	1.39	1.40	1.40	1.42
C2-C3	1.51	1.51	1.51	1.51	1.52
C3-O4	1.40	1.41	1.40	1.41	1.43
O4-C5	1.39	1.40	1.39	1.40	1.42
C5-C6	1.51	1.51	1.51	1.51	1.52
C6-O7	1.39	1.40	1.39	1.40	1.42
O7-C8	1.39	1.40	1.39	1.40	1.42
C8-C9	1.51	1.51	1.51	1.51	1.52
C9-O10	1.39	1.40	1.39	1.40	1.42
O10-C11	1.40	1.41	1.40	1.40	1.43
C11-C12	1.51	1.51	1.51	1.51	1.52
C12-O13	1.40	1.39	1.40	1.40	1.42
Na-Cl				2.69	2.72

Table 2.

Valence angle (grand) in optimized complexes of PEG4 polyethylene glycol with atoms of sodium, chlorine and NaCl ion pare

Angle	PEG4 and its complexes								
	PEG4 (HF)	PEG4+Na (HF)	Δ,°	PEG 4+Cl (HF)	Δ,°	PEG4+NaCl (HF)	Δ,°	PEG4+NaCl (B3LYP)	Δ,°
O_1-C_2-C_3	111.5	112.3	0.8	111.6	0.1	108.9	-2.6	108.9	0.05
C_2-C_3-O_4	107.3	110.4	3.1	107.6	0.3	108.5	1.2	108.3	-0.2
C_3-O_4-C_5	114.9	113.4	-1.5	114.8	-0.1	110.3	-4.6	123.5	13.5
O_4-C_5-C_6	109.4	109.7	0.3	109.7	0.3	108.6	-0.8	108.3	-0.3
C_5-C_6-O_7	109.3	108.5	-0.8	109.4	0.1	108.4	-0.9	108.1	-0.3
C_6-O_7-C_8	114.5	115.6	1.1	114.4	-0.1	115.3	0.8	114.3	-1.0
O_7-C_8-C_9	109.3	108.8	-0.5	109.4	0.1	107.4	-1.9	107.2	-0.2
C_8-C_9-O_{10}	109.4	109.7	0.3	109.7	0.3	111.1	1.7	111.7	0.6
C_9-O_{10}-C_{11}	114.9	113.5	-1.9	114.7	-0.2	116.6	1.7	115.4	-1.2
O_{10}-C_{11}-C_{12}	107.3	110.6	3.3	107.7	0.4	108.2	0.9	108.1	-0.1
C_{11}-C_{12}-O_{13}	111.5	112.3	0.8	111.6	0.1	109.2	-2.3	109.6	0.4

According to calculation results at PEG4+Na complex formation in comparison with PEG4 pure the increase of $C_2C_3O_4$ and $O_{10}C_{11}C_{12}$ angles on 3.1° and 3.3°, but insignificantly decrease of $C_3O_4C_5$ and $C_9O_{10}C_{11}$ angles on 1.5° and 1.9° are observed correspondingly. The formation of PEG4+Cl complex practically doesn't lead to change in PEG valence angle values except $C_2C_3O_4$, $O_4C_5C_6$ and $C_8C_9O_{10}$ angles which increase on 0.3° and change in $O_{10}C_{11}C_{12}$ angle doesn't exceed 0.4°. At complex formation with NaCl ion pare the most changes of $O_1C_2C_3$, $C_3O_4C_5$, $O_7C_8C_9$ and $C_{11}C_{12}O_{13}$ valence angles which decrease on 2.6°, 4,6°, 1,9° and 2.3° correspondingly. In optimization process $C_2C_3O_4$ and $O_{10}C_{11}C_{12}$ valence angles increase in comparison with pure PEG4 on 1.2°and 0.9° and $C_8C_9O_{10}$ and $C_9O_{10}C_{11}$ angles on 1.7° correspondingly. The calculation by B3LYP method in comparison with calculation by HF method leads to significant increase of $C_3O_4C_5$ valence angle on 13.5° whereas the changes in other valence angle values are insignificant ones (table 2).

Table 3.

Double-edge angles (grad) in of PEG4 polyethylene glycol with sodium and chlorine atoms and NaCl ion pare

Angle	PEG4 and its complexes				
	PEG4 (HF)	PEG4+Na (HF)	PEG4+Cl (HF)	PEG4+NaCl (HF)	PEG4+NaCl (B3LYP)
O_1-C_2-C_3-O_4	60.5	-65.9	60.8	57.4	56.4
C_2-C_3-O_4-C_5	-176.8	174.0	-176.3	169.4	169.4
C_3-O_4-C_5-C_6	-176.5	-174.9	-178.4	153.3	155.8
O_4-C_5-C_6-O_7	70.8	-60.7	69.7	54.0	52.5
C_5-C_6-O_7-C_8	-177.9	-170.2	177.1	177.4	178.8
C_6-O_7-C_8-C_9	177.9	173.1	-177.4	174.7	174.2
O_7-C_8-C_9-O_{10}	-70.8	61.5	-69.9	-59.6	-59.5
C_8-C_9-O_{10}-C_{11}	176.4	168.9	178.4	-93.6	-90.1
C_9-O_{10}-C_{11}-C_{12}	176.8	-174.8	176.2	177.6	178.0
O_{10}-C_{11}-C_{12}-O_{13}	-60.5	66.4	-61.0	-64.3	-64.5

From double-edge angles (table 3) at complex formation with NaCl ion pare angle $C_8C_9O_{10}C_{11}$ significantly changes on 107° which from straight angle (~180°) becomes direct one (~90°). C_3-O_4-C_5-C_6 double-edge angle changes on 30° and double-edge angles C_2-C_3-O_4-C_5, O_4-C_5-C_6-O_7 and O_7-C_8-C_9-O_{10} change on 14°, 17° and 11° correspondingly. According to all these changes in angle of inner rotation PEG4 cavity curls up round Na atom and becomes significantly more compact. The interatomic spaces between unbound oxygen atoms and sodium atoms, chlorine with oxygen and nearest hydrogen atoms in PEG4+NaCl complex are given in table 4 for more observable picture of changes which are observed in calculation process by different methods which are molecular dynamics and geometry optimization by HF and DFT/B3LYP methods.

Table 4.

Interatomic spaces (Å) between atoms of oxygen and sodium, chlorine with oxygen and nearest hydrogen in PEG4+NaCl complex

Complex PEG4+NaCl					
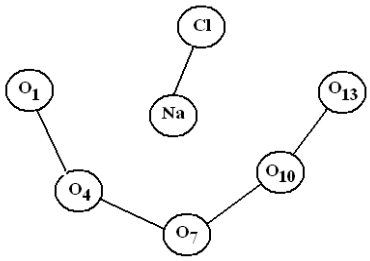		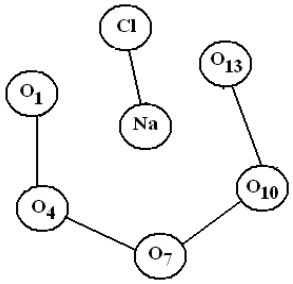			
Atoms	Molecular dynamics, bond length	Method HF		Method DFT/B3LYP	
		bond length	Δ	bond length	Δ
O_1-O_4	2.78	2.73	-0.05	2.74	0.01
O_4-O_7	2.62	2.68	0.06	2.69	0.01
O_7-O_{10}	2.87	2.77	-0.10	2.80	0.03
O_{10}-O_{13}	2.78	2.80	0.02	2.83	0.03
O_1-O_7	5.38	4.74	-0.64	4.77	0.03
O_1-O_{10}	6.59	5.19	-1.40	5.18	-0.01
O_1-O_{13}	7.31	3.77	-3.24	3.72	-0.05
O_4-O_{13}	6.59	4.59	-2.00	4.58	-0.01
O_7-O_{13}	5.38	4.33	-1.05	4.38	0.05
O_4-O_{10}	4.88	4.48	-0.40	4.50	0.02
Na-O_1	3.36	2.75	-0.61	2.70	-0.05
Na-O_4	2.74	2.43	-0.31	2.40	-0.03
Na-O_7	3.22	2.59	-0.63	2.60	0.01
Na-O_{10}	3.38	2.52	-0.86	2.55	0.03
Na-O_{13}	4.14	2.47	-1.67	2.45	-0.02
Cl –O_1	4.01	3.15	-0.86	3.06	-0.09
Cl -O_{13}	4.19	3.17	-1.02	2.45	-0.72
Na-Cl	2.53	2.69	0.16	2.72	0.03
Na-H_{14}	2.66	2.71	0.05	2.64	-0.07
Na-H_{16}	2.93	3.13	0.20	3.15	0.02
Na-H_{31}	3.45	2.51	-0.94	2.44	-0.07
Cl-H_{14}	3.58	2.33	-1.25	2.17	-0.16
Cl-H_{16}	3.88	3.14	-0.74	3.18	0.04
Cl-H_{31}	3.74	2.39	-1.35	2.17	-0.22

At PEG4 complex formation with NaCl ion pare the cavity forms, the stability of which is provided by interaction of oxygen atom of polyethylene glycol with sodium and hydrogen atoms with chlorine ones. The optimization by methods of molecular dynamic, HF and B3LYP leads to different values of bond lengths in NaCl ion pare which varies in limits from 2.53 Å up to 2.72 Å (table 4). The obtained data on Na approach with oxygen atoms and Cl with end atoms of oxygen and hydrogen of polyethylene glycol in optimization process agree with experimental investigation results, which confirm the fact of sodium cation coordination by ether oxygen atoms of polyethylene glycol. Chlorine anions are coordinated by PEG4 hydrogen atoms. According to calculation results Na is closer to end oxygen atom O_{13} on 1,7 Å and to O_1 and O_7 oxygen atoms it is closer on 0.6 Å. Cl atom after optimization by HF method approaches to oxygen end atoms H_{31} and H_{14} on 1.35 Å and 1.25 Å correspondingly and to end oxygen O_{13} on 1.02 Å. The most change has the distance between oxygen end atoms, which approach on 3.24 Å. If for example the interatomic space O_1 and O_{13} is 7.31 Å after optimization by HF method is 3.77 Å then calculations by B3LYP functional method evidence on biggest approach as a result of which the distance O_1-O_{13} is 3.72 Å. Thus, after optimization by HF method the coordination cavity becomes the more compact and narrow one. The interatomic spaces between oxygen atoms O_4-O_{13}, O_1-O_{10} and O_7-O_{13}, which decrease on 2.0 Å, 1.4 Å and 1.05 Å correspondingly, evidence on it. O_{13} (on 0.72 Å) and hydrogen atoms H_{31} и H_{14} (on 0.2 Å) are as a result of optimization by B3LYP method of more approached ones to chlorine atoms.

The dynamics of spatial variations taking place at PEG4 complex formation with NaCl ion pare in models

obtained by different methods is given on fig.2. In complex model obtained after molecular dynamics sodium atom is captured by only oxygen end atoms and the ion bond of sodium atom with chlorine atom, which comes forward from complex cavity upwards, remain constant (fig.2a).

The further structure optimization obtained by HF method (fig.2b) and later by B3LYP (fig.2, c) leads to such conformation reconstruction, at which sodium atom because of contacts with oxygen atoms of polyethylene glycol chain is surrounded by them from all sides in dense ring and is in the cavity middle whereas the chlorine atom interacting practically only with end hydrogen atoms goes out from the cavity moving away slightly from sodium atom. Moreover, as it is seen from fig.2, all neighboring hydrogen atoms turn to chlorine atom keeping it in formed complex. Such picture of polyethylene glycol complex formation with ion pare confirms the complex formation because of sodium cation interaction with oxygen atoms and chlorine anion interaction with polyethylene glycol hydrogen.

For quantitative comparison of changes taking place in PEG4 geometric parameters at different complex formation, one can analyze the calculation results integrated in table 5. For comparative analysis we used earlier studied PEG4 complexes with sodium and chlorine atoms and also results of present investigation. The interatomic spaces between unbound atoms of oxygen, sodium and chlorine as in pure PEG4 and in PEG4+Na, PEG4+Cl и PEG4+NaCl complexes calculated by HF/6-31G method are given in table 5.

As it is followed from table 5, at PEG4+Na complex formation the distance between O_1-O_{13} oxygen end atoms increases on 0,23 Å and non-adjusted inner oxygen atoms O_4 and O_{10} approach on 0,1 Å. The diagonally situated oxygen atoms O_4-O_{13} and O_1-O_{10} move away approximately on 0,1 Å.

Atom Na situates in PEF4 cavity like that distance between sodium atoms and oxygen inner atoms is less on 1,5 Å than between it and oxygen end atoms. Atom Na situates nearer to O_7 oxygen atom situating in cavity depth.

Moreover, the oxygen neighbor inner atoms approach on 0,1Å and distances between extreme oxygen pares O_1-O_4 and O_{10}-O_{13} increase on 0,13Å.

Thus, at atom Na fixation it situates symmetrically relatively O_4 and O_{10} oxygen atoms nearer to the cavity foundation of PEG4 insignificantly coming forward from complex cavity.

At PEG4+Cl complex formation the distances between whole neighbor pares of O_1-O_4, O_4-O_7, O_7-O_{10} and O_{10}-O_{13} oxygen atoms don't change. The most change in distance increase between oxygen end atoms O_1-O_{13} on 0,32 Å is observed.

The distance between inner discontiguous O_4 and O_{10} oxygen atoms increase on 0,12 Å and diagonally situated O_4-O_{13} and O_1-O_{10} oxygen atoms move away on 0,19 Å and 0,17 Å as if pulling apart the cavity for atom capture.

These geometric changes allow chlorine atom penetration in PEG4 cavity and location nearer to oxygen inner atoms O_4 and O_{10}.

The chlorine atom is on 0,4 Å from O_1 and O_{13} oxygen end atoms and is on 0,2 Å far away from O_7 atom situating in cavity depth.

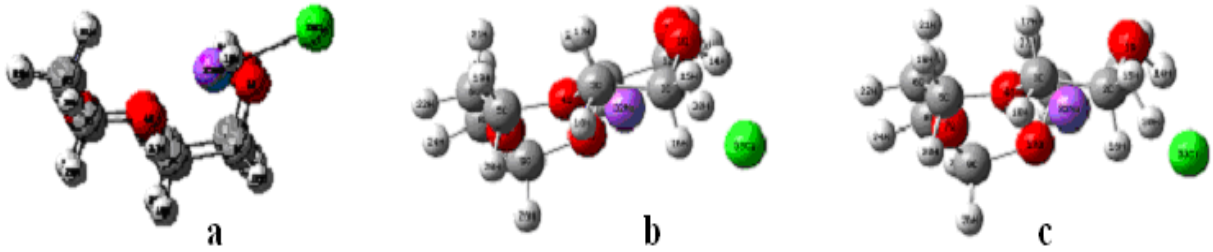

Fig. 2. The calculated models of polyethylene glycol complexes with NaCl ion pare (a) after molecular dynamics, b) after calculation by HF method; c) after calculation by DFT/B3LYP method)

In differences on PEG4+Na and PEG4+Cl complexes at complex formation PEG4+NaCl the distance between end oxygen atoms O_1-O_{13} in comparison with pure polyethylene glycol oligomer doesn't increase, as at PEG4 complex formation with sodium and chlorine, and significantly decreases on 3.54 Å; the cavity as if closes. The distance between O_1-O_7 oxygen atoms on 0,64 Å also significantly decreases. Such geometric changes form the more compact cavity. The distances between Na atom and oxygen end atoms strongly decrease. The distance between sodium atoms with O_{13} oxygen decreases on 1,57 Å and on 1,26 Å with O_1 oxygen in comparison with analogous distances in PEG4+Na complex. Thus, Na atom is strongly captured in cavity by oxygen end atoms. The distances between all neighbor oxygen atoms decrease besides O_{10}-O_{13}, the distances between which slowly increase on 0,02 Å. The distance between inner O_4-O_7 oxygen atoms decreases on 0.1 Å and becomes the same ones as in PEG4+Na complex.

The sodium atom situates nearer than others to O_7 oxygen central atom on distance 2.43 Å as in PEG4+Na complex, but in difference on PEG4+Na complex oxygen end atom O_{13} in PEG4+NaCl complex also strongly approaches to sodium atom on distance 2.47 Å.

In difference on PEG4+Cl complex in PEG4+NaCl complex chlorine atom nearer than others approaches to hydrogen end atoms H_{14} (2,33 Å) and H_{31} (2,37 Å) and oxygen end atoms O_{13} (2,47 Å) and O_1(3,15 Å) moving away from oxygen inner atoms.

The charges on atoms of PEG4 complex with NaCl ion pare and the charges on pure PEG4 atoms and its

complexes with sodium and chlorine for comparison and changes in charges taking place at formation of PEG4 complex with NaCl ion pare are given in table 6.

As it is seen from table 6 the most change in charge distribution at PEG4+Na complex formation is observed on O_7 (~0,05) oxygen atom and also on neighboring carbon atoms C_6 and C_8 (~0,04), C_2 and C_{12} (~0,016). At PEG4+Cl complex formation the changes in charge distribution are observed on the same atoms but they are practically insignificant ones (~0,005) that is explained by chlorine atom disposition not in PEG4 cavity but from the cavity situated above it . PEG4 formation complex with NaCl ion pare leads to charge decrease on all oxygen atoms, which become more electronegative ones. The most changes are observed on O_7 and O_4 (~0,03), O_{13}(~0,02) oxygen atoms. The charges on C_2 and C_9 carbon atoms also decrease on 0.034 and 0.028 charge units correspondingly. It is necessary to note that sodium has small negative charge (-0.161) in PEG4+Na complexes, the chlorine charge value is only (_0.003) in PEG4+Cl complex. At NaCl ion pare formation the sodium atom gives the electronic density to chlorine atom and the electrostatic attraction forces appear between formed Na^+ and Cl^- ions, as a result of which the ionic bond forms. That's why the sodium has big positive charge (0,610) in complex and chlorine has the big negative one (-0,779). The calculation by B3LYP method gives the essentially another picture of charge distribution, makes the oxygen atoms less electronegative and all carbon atoms of polyethylene chain have the negative charges. At comparison of calculation by DFT/B3LYP method with HF one, we observe that charges on C_2, C_5 and C_9 atoms decrease on 0,45 average and charges on C_3, C_6, and C_{12} atoms they decrease on 0,2 charge units. The charge more increases (on 0,3) on oxygen atoms being in cavity middle and charge is less by order (on 0,03) on end oxygen atoms.

The sodium charge atom at calculation by DFT/B3LYP method on 0,120 and chlorine atom on 0,145 charge units bigger than at calculation by above mentioned methods.

The stabilization of such type structures connects with interaction of negatively charged oxygen atoms and positively charged hydrogen atoms with positively charged sodium atom and negatively charged chlorine atom.

Table 5.

The interatomic spaces (Å) between atoms of oxygen, sodium and chlorine with oxygen atoms and neighboring hydrogen atoms in PEG4 complexes according to calculation data by HF/6-31G method.

PEG4 (HF)		PEG4+Na (HF)		PEG4+Cl (HF)		PEG4+NaCl (HF)	
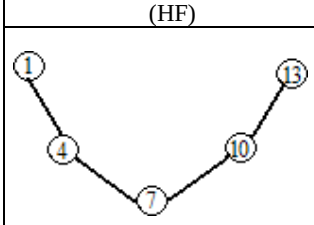		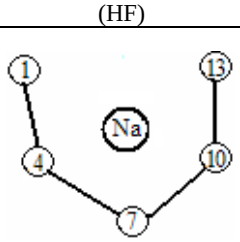		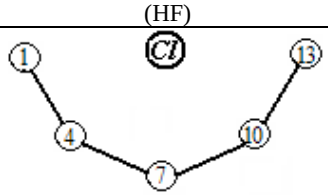		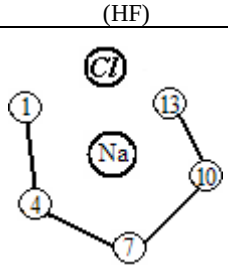	
O_1-O_4	2.78	O_1-O_4	2.91	O_1-O_4	2.79	O_1-O_4	2.73
O_4-O_7	2.87	O_4-O_7	2.78	O_4-O_7	2.87	O_4-O_7	2.68
O_7-O_{10}	2.87	O_7-O_{10}	2.77	O_7-O_{10}	2.87	O_7-O_{10}	2.77
O_{10}-O_{13}	2.78	O_{10}-O_{13}	2.90	O_{10}-O_{13}	2.79	O_{10}-O_{13}	2.80
O_1-O_7	5.38	O_1-O_7	5.36	O_1-O_7	5.38	O_1-O_7	4.74
O_1-O_{10}	6.59	O_1-O_{10}	6.67	O_1-O_{10}	6.76	O_1-O_{10}	5.19
O_1-O_{13}	7.31	O_1-O_{13}	7.54	O_1-O_{13}	7.63	O_1-O_{13}	3.77
O_4-O_{13}	6.59	O_4-O_{13}	6.69	O_4-O_{13}	6.78	O_4-O_{13}	4.59
O_7-O_{13}	5.38	O_7-O_{13}	5.38	O_7-O_{13}	5.39	O_7-O_{13}	4.33
O_4-O_{10}	4.88	O_4-O_{10}	4.80	O_4-O_{10}	4.98	O_4-O_{10}	4.48
		Na-O_1	4.01			Na-O_1	2.75
		Na-O_4	2.66			Na-O_4	2.43
		Na-O_7	2.43			Na-O_7	2.59
		Na-O_{10}	2.66			Na-O_{10}	2.52
		Na-O_{13}	4.04			Na-O_{13}	2.47
				Cl –O_1	3.90	Cl –O_1	3.15
				Cl –O_4	3.55	Cl –O_4	4.43
				Cl –O_7	3.69	Cl –O_7	5.16
				Cl -O_{10}	3.52	Cl -O_{10}	4.14
				Cl -O_{13}	3.88	Cl -O_{13}	2.47
				Cl-H_{14}	3.14	Cl-H_{14}	2.33
				Cl-H_{31}	3.11	Cl-H_{31}	2.39
						Na-Cl	2.69

It is known that electron transitions from ground state into excited one and reverse transitions take place constantly. The important processes: formation and change of color, absorption, reflection and dispersion of light and other radiations, many chemical reactions and etc. are connected with electron transitions. Two orbitals HOMO (Highest Occupied Molecular Orbital) and LUMO (Lowest Unoccupied Molecular Orbital) have the essential important meaning as approximately 98% of all electron transitions are the ones between orbitals of HOMO ground state and LUMO excited state. The many substance properties depend on energy difference between these two orbitals. The less the energy gap between these orbitals the easier one can dissociate the molecule. The energy values of HOMO and LUMO orbitals of pure PEG4 and PEG4 complexes with Na sodium atoms, Cl chlorine ones and NaCl ion pare in two HF/6-31G and DFT B3LYP/6-31G methods are given in table 7.

Table 6.

The charges on atoms in optimized PEG4 complexes

	PEG4	PEG4+Na		PEG4+Cl		PEG4+NaCl			
Atom	HF	HF	Δ c PEG4	HF	Δ c PEG4	HF	Δ c PEG4	B3LYP	Δ c HF
O_1	-0.649	-0.642	0.007	-0.651	-0.002	-0.656	-0.007	-0.621	0.035
C_2	0.104	0.088	-0.016	0.103	-0.001	0.070	**-0.034**	-0.370	-0.440
C_3	0.101	0.108	0.007	0.102	0.001	0.117	0.016	-0.106	-0.223
O_4	-0.653	-0.665	-0.012	-0.653	0.000	-0.679	**-0.026**	-0.408	0.271
C_5	0.122	0.125	0.003	0.123	0.001	0.120	-0.002	-0.311	-0.431
C_6	0.118	0.078	**-0.040**	0.114	**-0.004**	0.095	-0.023	-0.111	-0.206
O_7	-0.631	-0.677	**-0.046**	-0.635	**-0.004**	-0.660	**-0.029**	-0.387	0.273
C_8	0.118	0.082	**-0.036**	0.113	**-0.005**	0.102	-0.016	0.001	-0.101
C_9	0.122	0.123	0.001	0.123	0.001	0.094	**-0.028**	-0.384	-0.478
O_{10}	-0.653	-0.665	-0.012	-0.654	-0.001	-0.662	-0.009	-0.334	0.328
C_{11}	0.102	0.109	0.007	0.103	0.001	0.100	-0.002	-0.143	-0.243
C_{12}	0.104	0.088	-0.016	0.102	-0.002	0.086	-0.018	-0.370	-0.456
O_{13}	-0.649	-0.642	0.007	-0.651	-0.002	-0.670	**-0.021**	-0.646	0.024
Na		**-0.161**				0.610	0.771	0.730	0.120
Cl				-0.003		-0.779	-0.776	-0.634	0.145

Table 7.

HOMO and LUMO orbitals in optimized polyethylene glycol complexes

Complexes	PEG-4	PEG4+Na		PEG4+Cl		PEG4+NaCl	
Orbitals		α	β	α	β	α	α
Method	HF	HF	HF	HF	HF	HF	B3LYP
HOMO	-0.41878	-0.13158	-0.43322	-0.42050	-0.2270	-0.33863	-0.23175
LUMO	0.2865	0.04937	0.07001	0.22380	0.22521	0.09025	-0.02729
Δ	0.64743	0.18095	0.50323	0.64430	0.45221	0.42888	0.20446

Table 8.

Energy parameter and dipole moments of PEG4 and its complexes.

Energy parameter and dipole moment	PEG4	PEG4+Na	PEG4+Cl	PEG4+ NaCl (HF)	Δ (PEG4)	PEG4+ NaCl (B3LYP)	Δ (HF)
Total energy (RHF, au)	-687.708	-849.560	-1147.159	-1309.183	621.475	-1314.407	5.224
nuclear repulsion energy (Hartrees)	855.947	1031.893	1087.141	1347.197	491.250	1340.770	-6.393
Dipole moment (Debye)	4.778	10.085	4.755	10.954	6.146	10.561	-0.393

As it is seen the energy gap between HOMO and LUMO orbitals at PEG4 complex formation with chlorine atom practically doesn't change and at complex formation with sodium it strongly decreases for α-electrons.

The energy gap decreases on 0,21855 units at PEG4 complex formation with NaCl ion pare. This value more decreases on 0.22442 units at B3LYP calculation.

The energy parameters and PEG4 dipole moments, its complexes are given in table 8.

As it is followed from calculation results at Na fixation of PEG4+Na complex energy decreases in comparison with pure PEG4 on 162 atomic units, dipole moment increases on 5.3D, at chlorine fixation of PEG4+Cl complex decreases on 459 atomic units forming more compact structure, dipole moment decreases on 0,023D. At PEG4 complex formation with NaCl ion pare the total complex energy decreases on 621at.un. in comparison with pure oligomer PEG4. This complex is more energy-advantageous one than PEG4 and PEG4 complexes with isolated atoms of sodium or chlorine. The dipole moment of PEG4+NaCl increases on 6.146D but cavity structure becomes most compact one

from all complexes under consideration. The total energy decreases only on 5.224 at.un. and dipole moment decreases on 0.4D at calculation by DFT method with B3LYP hybrid functional.

Thus, PEG4 polyethylene glycol oligomers are inclined to fixation of sodium or chlorine atoms but especially to fixation of NaCl ion pare, as such complex-formation leads to energy structure stabilization and most quantity of fixation contacts (interactions) of oxygen atoms with sodium cation and chlorine anion with hydrogen end atoms.

[1] *M.O. Durimanov, A.B. Ulasov, E.A. Belechkaya, N.S. Rodichenko, Yu.B. Rozenkranch, Yu.B. Xramchov, A.A. Rozenkranch, A.S. Sobolev.* Nanochastitsi polipleksov s ligandom dlya dostavki genov v rakovie kletki melanomi. IV syezd biofizikov Rossii. Simpozium I "Fiziko-khimicheskie osnovi funktsionirovaniya biopolimerov i kletok", Nijniy Novgorod, 2012, Materiali dokladov, s.80. (In Russian).

[2] *J. Chen, S.K. Spear, J.G. Huddleston, R.D. Rogers.* Green Chem., 2005, vol.7, No.2, p.64-82.

[3] *J. Chen, S.K. Spear, J.G. Huddleston, J.D. Holbrey, R.P. Swatloski, R.D. Rogers.* Ind. End.Chem.Res., 2004, vol. 43, No.17, p.5358-5364.

[4] *M.B. Kosevich, V.G. Zobnina, E.N. Jivotova, I.V. Shiqol, O.A. Boryak, V.V. Chaqovets, V.V. Chekanova, A.V. Zinchenko, V.A. Pokrovskiy, A. Gomori.* Mass spektrometriya. 2009, 6, № 1, s. 7-20. (In Russian).

[5] *J. Gidden, T. Wyttenbach, A.T. Jackson, J.H. Scrivens, M.T. Bowers.* J. Am. Chem. Soc., 2000, Vol. 122, No. 19, p. 4692–4699.

[6] *A.T. Jackson, J.H. Scrivens, J.P. Williams, E.S. Baker, J. Gidden, M.T. Bowers.* Int. J. Mass Spectrom., 2004, vol. 238, No. 3, p. 287–297.

[7] *T. Wyttenbach, G. von Helden, M.T. Bowers.* Int. J. Mass Spectrom. Ion Proc. 1997, 165/166, 377-390.

[8] *K. Shimada, S. Matsuyama, T. Saito, S. Kinugasa, R. Nagahata, S. Kawabata.* Int. J. Mass Spectrom., 2005, vol. 247, No. 1–3, p. 85–92.

[9] *Y. Yokoyama, R. Hirajima, K. Morigaki, Y. Yamaguchi, K. Ueda.* J. Am.Soc. Mass Spectrom., 2007, vol. 18, No. 11, p. 1914–1920.

[10] *V.G. Zaikin.* Mass-spektrometriya sinteticheskix polimerov. M.: VMSO, 2009, 332 s. (In Russian).

[11] *Van L.E. Vlerken, T.K. Vyas, M.A. Mansoor.* Pharm. Res., 2007, vol. 24, No. 8, p. 1405–1414.

[12] *V.V. Chagovets, V.G. Zobnina, M.V. Kosevich.* Konferentsiya molodikh uchenikh "Fizika nizkikh temperatur", Xarkov, 1-5 iyunya 2009, s.95. (In Russian).

[13] *V.G. Zobnina, M.V. Kosevich, V.V. Chagovets, O.A. Boryak, A.N. Kulik, Gomori Aqnesh.* Mass Spectrom, 2010, t. 7, № 3, c.225-231. (In Russian).

[14] *G.I. Kobzev.* Primenenie neempiricheskikh metodov v kvantovo-khimicheskikh raschetax. Orenburg, 2004, 146 s. (In Russian).

[15] *S.D. Demukhamedova, Z.I. Hadjiev, I.N. Alieva, N.M. Godjaev.* Resp. nauchno-prakticheskaya Konf. «Opto-, nanoelektronika i fizika visokikh energiy», Baku, 2012, s. 234-237. (In Russian).

[16] *Z.I. Hadjiev, S.D. Demukhademova, I.N. Alieva, N.M. Godjaev.* Journal of Gafgaz University, Physics, 2013,vol.1, № 1, s.40-46. (In Russian).

[17] *S.D. Demukhamedova, Z.I. Hadjiev, I.N. Alieva, N.M. Godjaev.* Opto-, nanoelektronika kondensə olunmuş mühit və yüksək enerjilər fizikası" VII Respublika elmi-praktik konfransı, Bakı, dekabr, 2013.

[18] *S.D. Demukhamedova, Z.I. Hadjiev, I.N. Alieva, N.M. Godjaev, L.A. Nurieva.* Ist International scientific conference of young researchers, Proceedings, Gafgaz University, 26-27 aprel 2013, Baku, Azerbaijan, p.250-252.

Received: 23.10.2014

EPITAXIAL GROWTH ON SUPERSTRUCTURAL CELLS OF $YbAs_4Se_7$ THIN FILMS

E.Sh. HAJIYEV
Institute of Physics, Academy of Sciences of Azerbaijan, 33 H. Javid, Baku Az – 1143, Azerbaijan
elmanhaji@mail.ru

The conditions growth of thin films of $YbAs_4Se_7$ obtained vacuum deposition has been defined using electron diffraction method. It is established epitaxy relations existing between long periodic superstructure phases and initial structures.

Keywords: electron diffraction, epitaxial growth, thin films.
PACS: 61.05.J, 68.55.-a, 81.15.Aa

INTRODUCTION

Due to the significant progress in the development and creation of new technological and functional semiconductor materials, significantly increased interest in the methods of preparation of multicomponent nanostructure semiconductor compounds. Ultra thin films of these compounds, which pays special attention to belong to the so called size-limited (at least in one dimension) structures, the role of which is dominant in creating the foundation of functional nanoelectronics. Physical properties of materials in confined geometry differ significantly from the properties of bulk materials. It is known that if one of three dimension values of a solid body is comparable with some characteristic physical parameter ones (size of the magnetic domains, length of free run of electron, an electron de Broglie wavelength, etc.), then the observed dimensional effects lead to relevant properties which can lead to considerable modification and even noticeable change of bulk semiconductor compound properties. Large possibilities in modification of properties of classic materials, in creation of new compositions with unique descriptions are opened with development of materials science films and use thin-film nanotechnology.

EXPERIMENTAL RESULTS AND DISCUSSION

In this paper we present the results of electron diffraction studies of formation conditions of $YbAs_4Se_7$ thin films with different substructure obtained by vacuum deposition.

$YbAs_4Se_7$ of ~ 30 nm film thickness are prepared by evaporation of the synthesized substance and deposited with 5.0 nm/sec rate on NaCl, KCl, NaBr, LiF, KJ crystals and celluloid. At room temperature $YbAs_4Se_7$ films form in the amorphous state. Obtained by variable exposure the electron diffraction pattern of $YbAs_4Se_7$ amorphous film shows five diffuse rings corresponding to the values S= 14.15, 29.00, 48.50, 77.50, 101.0 nm^{-1} (Fig. 1). Prolonged storage of the amorphous films at room temperature does not lead to spontaneous crystallization.

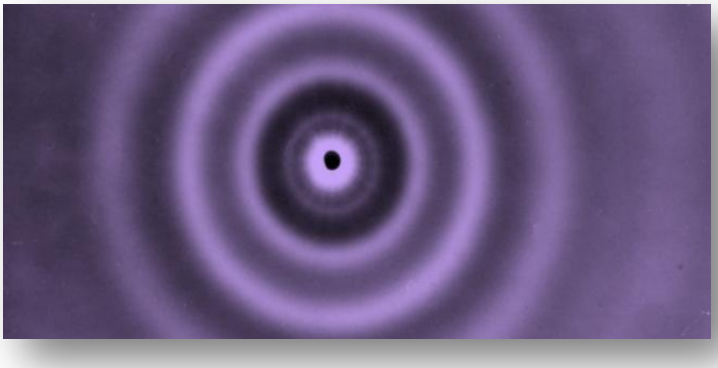

Fig.1. Electron diffraction pattern of $YbAs_4Se_7$ amorphous films.

Heating the $YbAs_4Se_7$ amorphous layers at 363 K resulted in the formation of the crystalline phase orthorhombic modification. Polycrystalline films diffraction pattern from which indicate based orthorhombic crystal lattice parameters:

a = 1,198; b = 1,470; c = 0,410 nm, as obtained by preheated in a substrate temperature range 373 - 513K. (Fig. 2).

On the electron diffraction pattern from the films produced on substrates of KJ with surface temperature 518K, are observed a mixture of polycrystalline and single crystal. The analysis of these electron diffraction patterns shows two-phase. The mixture of polycrystalline samples with a mosaic single crystal is formed in the range of the LiF substrate temperatures from 518 to 523K (Fig. 3).

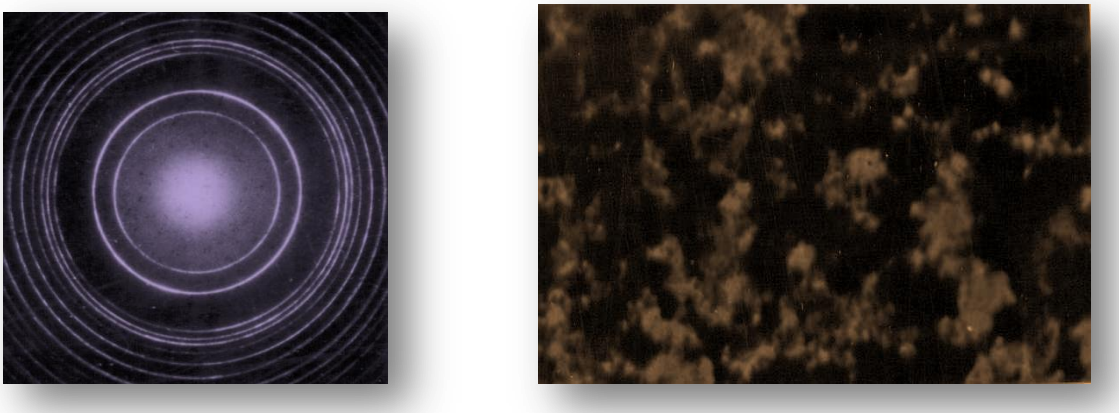

a b

Fig.2. a) electron diffraction pattern of $YbAs_4Se_7$ polycrystalline films, b) microstructure of the $YbAs_4Se_7$ surface layer (x 15000)

On the electron diffraction pattern from the films produced on substrates of KJ with surface temperature 518K, are observed a mixture of polycrystalline and single crystal. The analysis of these electron diffraction patterns shows two-phase. The mixture of polycrystalline samples with a mosaic single crystal is formed in the range of the LiF substrate temperatures from 518 to 523K (Fig. 3).

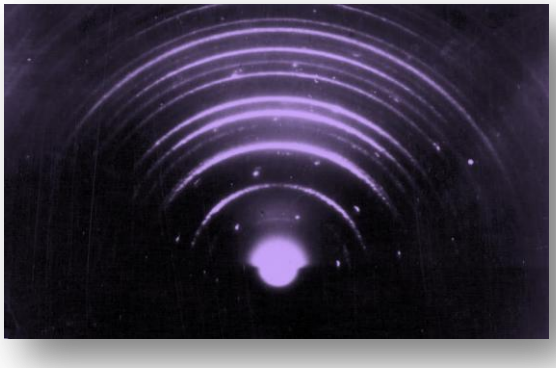

Fig.3. Electron diffraction pattern of polycrystalline samples with a mosaic single crystal.

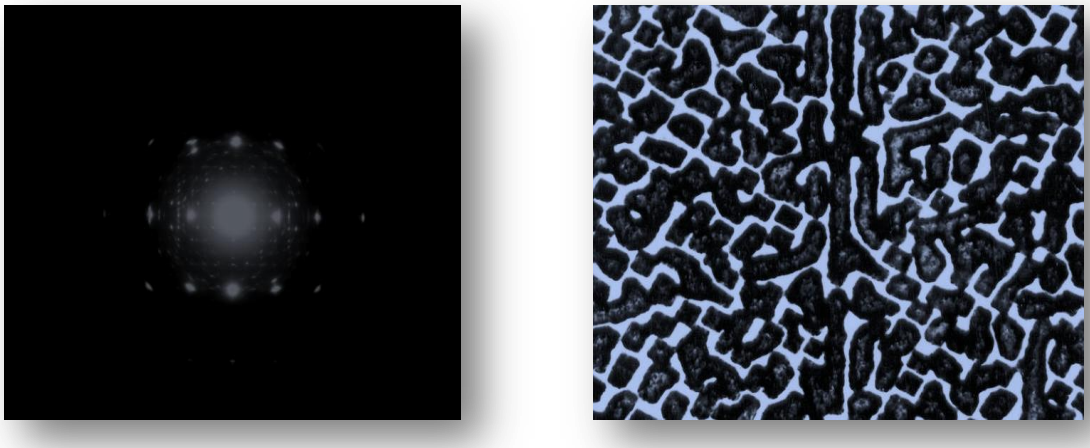

a) b)

Fig.4. Electron diffraction pattern (a) from single crystal superstructure phase and (b) microstructure of the surface of $YbAs_4Se_7$.

$YbAs_4Se_7$ films grown on hot substrates (T_s = 523K) are monocrystalline, but do not repeat the geometry of the substrate. The electron diffraction pattern taken at different points of the area of the same film exhibit spotlights reflexes not obey, but no laws, and on which it is impossible to determine the unit cell and make indexing reflections - achieve unambiguous identification. We experimentally found that obtaining thin films of $YbAs_4Se_7$ compound passing into the superstructure condition possible on substrates consisting of freshly cleaved KJ single crystal preheated to a temperature of 528K. Further the samples were annealed at a temperature of 538K for 2 hours in a vacuum of $\sim 10^{-4}$ Pa.

Electron diffraction patterns obtained from these films are displayed in the orthorhombic cell with parameters: $a_{sv.str.} \approx 3a_o$ = 3.594; $b_{cv.str.} \approx 2b_o$ = 2.934 nm; $c_{sv.str.} \approx 4c_o$ = 1,641 nm.

$YbAs_4Se_7$ monocrystalline films are also formed on the LiF substrates at a temperature of 558K. According to the law of the extinction of a reflexes the electron diffraction pattern obtained from single crystal superstructure phase $YbAs_4Se_7$ is described ASG $P222_1$ (D_2^2).

Electron diffraction pattern from single crystal superstructure phase and microstructure of the surface of $YbAs_4Se_7$ is shown in Figure 4.

CONCLUSION

We installed superstructure lattices oriented planes (100) parallel to the (100) LiF. During epitaxial growth of $YbAs_4Se_7$ thin films one unit cell superstructure phase interfaces with multi-cell substrate LiF. The relative mismatch of interfaced nets for pair $YbAs_4Se_7$ is about 2.1%.

---

[1] *E.H. Efendiyev, E.Sh. Hajiyev* Structural parameters of new amorphous semiconductors films of Yb-As-S(Se,Te) systems 25-th International Conference on Physics of semiconductors, Osaka, Japan, sept. 2000.

[2] *E.Sh. Hajiyev.* Short – range order parameters in amorphous $YbAs_4X_7$ (X-S, Se,Te) films International conference, Fizika-2005, June 7-9, Baku, Azerbaijan, p. 198-200.

[3] *E.Sh. Hajiyev, A.I. Madadzade*. Kinetika kristallizatsii amorfnikh plenok As_4Se_7. Izv.AN Azerb. Ser.fiz.-tekhn. i mat. Nauk, XXVI, 2006, №5, s.124 – 126. (in Russian).

[4] 19th International Conference on Ternary and Multinary Compounds (ICTMC-19), September 1-5, 2014, Niigata, Abstract Number: 1186946.
Corresponding Author: Elman Sh. Hajiyev.
Title: $YbAs_4Se_7$ thin films epitaxially growth.

Recevied: 12.11.2014

STRUCTURAL AND OPTICAL CHARACTERIZATION OF NANOSTRUCTURED CdS THIN FILMS DEPOSITED BY SPRAY PYROLYSIS METHOD

Z.Q. MAMIYEV, N.O. BALAYEVA, N.M. FATHI, A.M. KERIMOVA, Y.N. ALIYEVA, N.A. QASIMOV, A.H. BAYRAMOV

Institute of Physics of ANAS named by G.M. Abdullayev, AZ-1143, Baku, Azerbaijan

E-mail: bayramov@physics.ab.az

Influence of solution pH on the structural and optical properties of CdS films deposited by conventional spray pyrolysis technique was studied. X-Ray Diffraction (XRD), Atomic Force Microscopy (AFM), Photoluminescence spectroscopy and Spectroscopic Ellipsometry (SE) methods were used for the characterization of the films. The difference in the properties of the films was analyzed in terms of variation of grain sizes of the films.

Keywords: cadmium sulfide, spray pyrolysis, thin films, optical band gap.
PACS: 6855 Jk.

1. INTRODUCTION

Cadmium sulfide (CdS) thin films are widely used as universal window layers in thin film solar cells based on the different active-layer materials such as cadmium telluride (CdTe) [1,2], copper indium diselenide (CIS) and copper indium gallium diselenide (CIGS) [3,4]. CdS has a band-gap of 2.42eV which causes considerable absorption of sunlight in the short wavelength region. Extending transparency of a window material into a region above the energy gap of CdS may provide increased efficiency of solar cells. X.Wu [2] has reported the improvement of the conversion efficiency of CdTe solar cells when CdS film was deposited on CdTe by rf sputtering in the presence of oxygen at room temperature. According to the report [2], the prepared nanostructured CdS:O films had higher band-gap, as compared with bulk CdS which improved the quantum efficiency of solar cells in the short wavelength region.

Structures and optical properties of CdS:O films deposited at different oxygen partial pressures by rf magnetron sputtering were examined in [5]. It was shown that CdS:O thin films obtained under partial oxygen pressure below 3 % have crystal structure of bulk CdS, while above 3% show an amorphous structure. An increase in transparency of the CdS:O (5%) in short wavelength region was attributed to several factors including redistribution of the density of states in amorphous CdS, quantum size effect in nano-crystals of CdS, and contribution of amorphous CdO_2.

In this work the attempt of preparation of nanostructured CdS thin films by spray pyrolysis method was made. The preliminary results of structural and optical characterization of the films are given.

2. EXPERIMENTAL DETAILS

The CdS films were prepared by the spraying of aqueous mixture of cadmium acetate CdAc2 (0.025M) and thiourea $(NH_2)_2CS$ (0.025 M) and ammonium acetate $(NH_4)Ac$ onto heated up to 400 ^{0}C soda lime glass substrates. NH_4OH was added to the mixture to increase of pH of the solution. Three types of CdS films were deposited from different solutions with initial pH of 6.7; 9.5 and 10.2.

X-Ray diffraction (XRD) analyses of the films were carried out using Bruker D2 Phaser (Germany) diffractometer in θ-2θ scan mode with Ni-filtered CuKα radiation (λ=1.54060 Å) source.

Topography analysis of the thin films was performed in Smart SPM 1000 AIST NT (Tokyo Instruments, Japan).

Photoluminescence (PL) measurements were performed using standard spectrometer LS-55 (Perkin-Elmer, USA). The samples were excited by the 400 nm line of xenon lamp.

The ellipsometric measurements in 220-1700 nm spectral range were performed using Woollam M2000 (USA) rotating compensator instrument. Incident light angles were varied between 50 and 60° with 5° step. WVASE32 computer program was used for the ellipsometric data fitting procedure. Experimental data were fitted (employing the Levenberg–Marquardt algorithm) to optical model using parameterized model dielectric functions simultaneously for all the data points measured in UV/VIS ranges.

All of the measurements were performed at room temperature.

3. RESULTS AND DISCUSSION

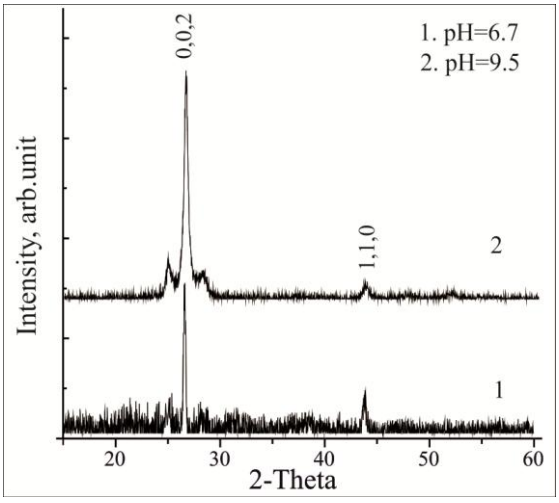

Fig.1. The x-ray diffraction spectra of CdS thin films prepared at 1) pH=6.7, 2) pH=9.5.

The XRD patterns of the CdS sample deposited from the solution with pH=6.7 and pH=9.5 exhibit prominent broad peaks at 26.7˚ and 44˚ which can be attributed to hexagonal wurtzite structure (PDF 01-074-9663) with p63mc space group and lattice parameters a=4.136, c=6.716 (Fig.1).

The films have highly oriented crystallites with a preferential orientation along the c-axis (002) perpendicular to the substrate plane. CdS films deposited from the solution with pH=10.2 shows very weak reflection and has nearly amorphous structure.

The crystallinities (crystallization degree), average grain sizes and dislocation densities of the films derived from the XRD data are summarized in Table 1.

The average grain sizes of the polycrystalline films were calculated by the Scherrer equation,

$$D = \frac{\alpha\lambda}{\beta cos\theta}$$

where D is the average grain size, α is constant (equal to 0,9), λ is the X-Ray wavelength (1.54060 Å), β is full width at half maximum (FWHM) of the diffraction peaks. The crystallinities were calculated from XRD patterns of the films using DIFFRAC.EVA.V2.1 PC program.

Dislocation density δ of the CdS thin films is defined as the length of dislocation line per unit volume of the crystal and can be determined using the relation [6].

$$\delta = \frac{1}{D^2}$$

where D is the average grain size.

Table.1

Crystallinity, average grain size and dislocation density of CdS films

Samples	Crystallinity, %)	Average grain size, (nm)	Dislocation density (δ)
CdS (PH)=6.7	28.7	20.4	2.40×10^{9}
CdS (PH)=9.5	~11.5	10	8.26×10^{9}
CdS (PH)=10.2	Weak reflection	<10	-

As it's seen from the table 1, the structural properties of the CdS thin films strongly depends on deposition conditions. The crystallinities and average grain sizes of the films decrease while the dislocation densities increase with pH of the reaction solution.

AFM measurements were performed to study the surface morphology of the CdS thin films deposited at different pH consentration. Fig.2 illustrates the AFM images of the films deposited from the solution with pH=6.7 and pH=9.5. Scanning area is 10×10 μ^2. As it is seen from the Fig. 2, the AFM measurement results are in good agreement with XRD data. The surface roughness (RMS) of the films increases with pH of the solution and are 4.63 nm and 8.62 nm for the films with pH=6.7 and pH=9.5, respectively.

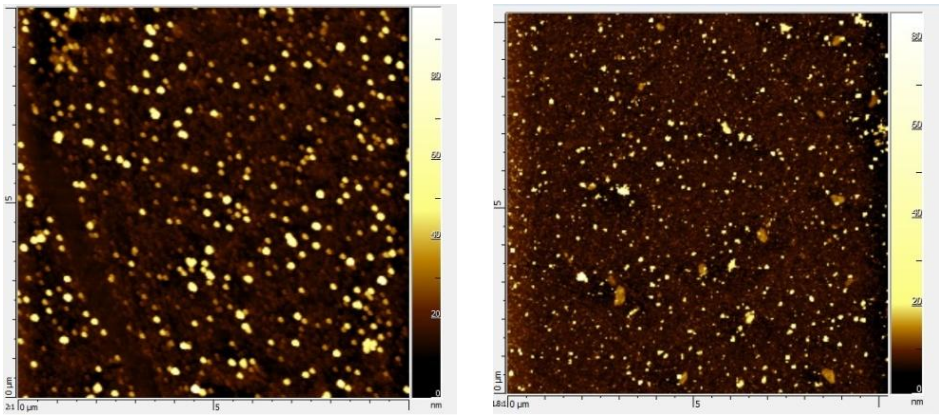

a) **b)**

Fig.2. Surface morphology of CdS thin films a) pH=6.7, b) pH=9.5.

The photoluminescence measurements were used to study the optical properties of the deposited thin films (Fig. 3). PL spectrum of CdS film deposited from the solution with pH=6.7 shows two bands at 520 nm and 600 nm caused by band to band and defect center transitions, respectively (Fig.3, curve 1). But PL spectrum of the film deposited from the solution with pH=10.2, except for these bands, shows also broad band PL emission located at 460 nm (2.7 eV) (Fig.3, curve 2). This emission can be attributed to peak shift of the band-to band emission of nanostructured CdS films due to the quantum size effect at grain sizes of < 10 nm.

Spectroscopic ellipsometry measurements were performed to reveal the quantum size effect in nanostructured CdS films deposited from the solution with pH=10.2 pictured in Fig.4. The real ε_1(curve 1) and imaginary ε_2 (curve 2) parts of dielectric function of the film are shown in Fig. 4.

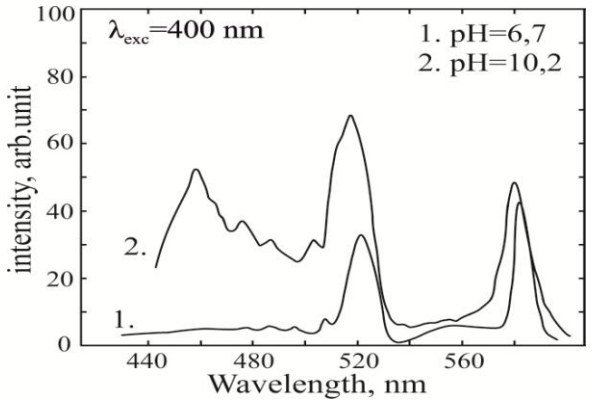

Fig.3. PL spectra of CdS thin films, 1) pH=6.7, 2) pH=10.2.

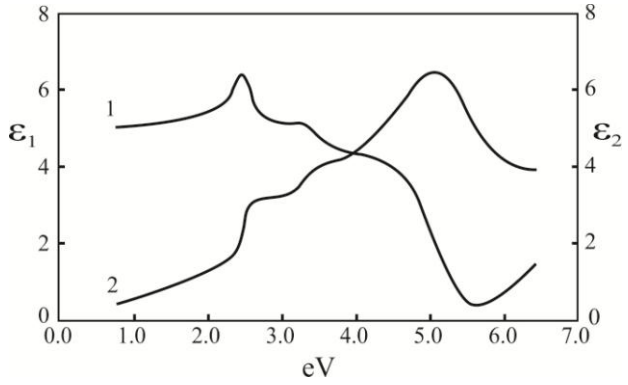

Fig.4. Real ε_1 (curve 1) and imaginary ε_2 (curve 2) parts of dielectric function of CdS film with pH=10.2.

Two transitions can be observed in these spectra: the first transition at about 2.4 eV is due to the absorption at the fundamental band gap of CdS and the second one above 4.5 eV represents the transitions along the Γ→A direction of the Brillouin zone of the hexagonal CdS lattice [7]. As opposed to luminescence spectra, no shifts of ε_1 and ε_2 due to the quantum size effect are observed in dielectric function spectra and energy band gap at the critical points of the electronic band structure of CdS are not affected by the increased pH of the solution. The possible reason of this can be low concentration of nanostructured CdS centers, which are well manifested in luminescence of the films, but not in dielectric function spectra, because density of state of these centers are negligible in comparison with the density of states at the fundamental band gap of bulk CdS.

4. CONCLUSION

Grain sizes of CdS thin films deposited by spray pyrolysis method decrease with increase of pH of reaction solution. PL spectrum of the film deposited from the solution with pH=10.2 shows broad band PL emission located at 460 nm (2.7 eV) which can be attributed to the quantum size effect at grain sizes of < 10 nm. No shifts of ε_1 and ε_2 due to the quantum size effect are observed in dielectric function spectra what can be caused by low concentration of nanostructured CdS centers, and therefore negligibility of density of state of these centers in comparison with the density of states at the fundamental band gap of bulk CdS.

[1] *J. Britt and C. Ferekides*, Appl. Phys. Lett., 1993, **62**, 2851.
[2] *X. Wu.*Sol. Energy, 2007, **77**, 803.
[3] *K. Ramanathan, M.A. Contreras, C.L. Perkins, S. Asher, F.S. Hasoon, J.Keane, D.Young, M. Romero, W.Metzger, R.Noufi, J.Ward, and A. Duda,* Prog. Photovolt., Res. Appl. 2003, **11** , 225.
[4] *K. Ramanathan, G. Teeter, J. C. Keane, and R. Noufi.* Thin Solid Films, 2005, **480-481**, 499.
[5] *Ryo Asaba, Kazuki Wakita, Atsushi Kitano, YongGu Shim, Nazim Mamedov,Ayaz Bayramov, Emil Huseynov, and Ilham Hasanov*. Phys. Status Solidi **C 10**, 2013, No. 7–8, 1098–1101.
[6] *M.A. Islama, M.S. Hossain, M.M. Aliyu.* Energy Procedia, 2013, **33**, 203 – 213.
[7] *H. Kanazawa and S. Adachi*. Optical properties of wurtzite CdS. Journal of Applied Physics, 1995. **78**, 1183-1190.

Received: 11.11.2014

THERMOELECTRIC PROPERTIES OF $TlInTe_2$-$TlYbTe_2$ SYSTEM SOLID SOLUTION

A.M. AHMEDOVA G.H. ISMAYILOVA
Sumgait State University

The work has been dedicated to the researching thermo-effecting of the solid solution $TlInTe_2$-$TlYbTe_2$. It was found out that when the relative quantity of the itterbium in solid solution $TlIn_{1-x}Yb_xTe_2$ rises, electric conducting increases. As the result of additional separation heating conducting coefficient was acute reduced. As a result it was caused the rising of the thermo effective coefficients' of the same contents.

Keywords: electric conduction, thermal conduction, single crystal.
PACS: 07.20.Dt, 64.75.Nx

The work is dedicated to investigation of $TlInTe_2$-$TlYbTe_2$ solid solutions thermo-efficiency. It is revealed that electric conduction increases almost in two times in $TlIn_{1-x}Yb_xTe_2$ solid solutions with ytterbium content increase in compositions, and thermal conduction coefficient significantly decreases because of additional center appearance of phonon scattering and these circumstances lead to thermal efficiency increase of the given compositions.

The interaction in Tl-$InTe_2$-$TlYbTe_2$ system from which it is followed that $TlInTe_2$-$TlYbTe_2$ section is quasi-binary one of quadruple system Tl-In-Yb-Te_2 is investigated in refs [2-4]. The quadruple compound $Tl_2InYbTe_4$ is formed at equal ratio of initial components 1:1 and solid solutions $TlIn_{1-x}Yb_xTe_2$ which are crystallized in tetragonal cell as $TlInTe_2$ initial compound are formed on the base of $TlInTe_2$ initial compound.

The solid solutions of bismuth telluride (*n*- branch) and stibium (*p*- branch) are used for thermoelectric cooling. The polycrystalline materials obtained mainly by zone melting are applied for preparation of thermo-coolers.

Last time the micro-miniaturization problem has the bigger development in connection of which the definite requirements to thermo-element branch materials and especially high degree homogeneity, well mechanical strength, structure perfection, high thermoelectric parameters.

Polycrystalline materials haven't already satisfied many of these requirements. From this point of view the monocrystalline samples of $TlIn_{1-x}Yb_xTe_2$ solid solutions present the special interest.

The samples are obtained from Tl, In, Te elements "e.p" (especial pure) and Yb "ch.p." (chemical pure) by direct synthesis in evacuated quartz ampoules up to 10^{-2} Pa. The stove is heated up to 1200-1300K in the dependence on mixture composition, is endured at this temperature 10-12 h and after is cooled up to room temperature with velocity 1012km/h. The alloys are annealed at 900-1100K during 140-180h for equilibrium state obtaining.

The single crystals are grown up in quartz ampoules with inner diameter 9-12mm and length 110mm, crystal growth has been continued 4 days. The obtained crystals are cut on two plane-parallel mirror cleavage planes.

The presence of big concentration $(\sim 10^{19} - 10^{20} см^{-3})$ of stoichiometric vacancy in crystal lattice of $TlIn_{1-x}Yb_xTe_2$ solid solutions and localized states in forbidden band [2] connected with them, is the character peculiarity of solid solutions. This value increases with mole rate increase in solid solution content as a result of which the electric conduction significantly increases (almost in two orders) with increase of ytterbium content in $TlIn_{1-x}Yb_xTe_2$ solid solution composition, electric conduction coefficient decreases because of appearance of additional of phonon scattering and these circumstances lead to increase of thermo-efficiency of the given compositions [2].

Thermo-electric effect is carried out on equation base

$$z = \alpha^2 \sigma / \chi \qquad (1)$$

(where is thermo-emf, $\sigma -$ is electric conduction coefficient, $\chi -$ is thermal conduction coefficient).

The calculations show that at temperatures 500-900K in some compositions the thermo-efficiency is $(2{,}44 \div 3{,}21)10^{-3}$ K^{-1}. The biggest value of thermo-efficiency in given temperature interval has the composition $TlIn_{0,91}Yb_{0,09}Te_2$ (see table).

Table

Thermoelectric efficiency of $TlIn_{1-x}Yb_xTe_2$ solid solutions

Compositions	500 K				600 K				800 K			
	α, 10^{-6} V/K	σ cm/m	χ $W/(m\cdot K)$	z, 10^{-3} K^{-1}	α, 10^{-6} V/K	σ cm/m	χ $W/(m\cdot K)$	z, 10^{-3} K^{-1}	α, 10^{-6} V/K	σ cm/m	χ $W/(m\cdot K)$	z, 10^{-3} K^{-1}
$TlIn_{0.99}Yb_{0.01}Te_2$	680	540	0.91	0.3	675	800	0.74	0.67	590	1500	0.71	1.1
$TlIn_{0.95}Yb_{0.05}Te_2$	670	1210	0.48	1.13	686	810	0.45	0.8 5	560	930	0.42	0.69
$TlIn_{0.93}Yb_{0.07}Te_2$	660	1400	0.46	1.32	675	820	0.44	0.85	550	910	0.40	0.69
$TlIn_{0.91}Yb_{0.09}Te_2$	650	1700	0.38	1.80	690	2500	0.37	3.21	540	2850	0.34	2.44

[1] *M.M. Zarbaliyev, N.F. Gaxramanov, A.M. Axmedova, A.B. Maqerramov.* Izvestiya AN Azerb. Respub. Seriya fiz-mat. i tekh. Nauk. 2010, № 5. (in Russian).

[2] *M.M. Zarbaliyev, E.G. Mamedov, A.M. Akhmedova, G.I. Zeynalov.* Teploprovodnost tverdikh rastvorov $TlIn_{1-x}Dy_xTe_2$. Dokladi RAN, Neorganich. materiali. 2007, t. 43, №12, s. 1432-1435. (in Russian).

[3] *M.M. Zarbaliyev.* Tverdie rastvori zamesheniya v sisteme $TlInTe_2 - TlYbTe_2$. Dokladi RAN, Neorganich. materiali. 1999. t.35. №5, s.560-564. (in Russian).

[4] *M.M. Zarbaliyev.* Yavlenie perenosa zaryada i tepla v sistemax $TlInS_2(Se_2, Te_2) - TlLnS_2(Se_2, Te_2)$. – Avtoreferat dissertatsii na soiskanie uch. stepeni doktora fiz.-mat. nauk, Baku, 2001. (in Russian).

Received: 15.09.2014

ELECTRIC PROPERTIES OF LDPE-CdS NANO-COMPOSITES ON THE BASE OF PRE- IRRADIATED POLYMER

M.A. NURIYEV, A.M. MAGERRAMOV, A.A. SHUKUROVA, I.M. NURUYEV
Institute of Radiation Problems of ANAS
AZ 1143, F. Agayev str., 9, Baku, Azerbaycan

The electric properties of LDPE/CdS nano-composites obtained by method of film oriented stretching previously modified by γ-irradiation influence have been investigated. It is shown that changes in nano-composite dependences $\rho v=f(1/T)$ with modification different doses by previous γ-irradiation are the result of molecular segment mobility difference of oriented crazed regions and differences of radiation process velocities in the structure of oriented polymer matrix.

HDPE/CdS nano-composite thermo-treatment leads to stabilization of structural and energy states of charge carrier active centers because of filler penetration into matrix volume.

Keywords: composite, low-density polyethylene, oriented stretching, γ –irradiation, electric properties, resistivity, molecular segment, mobility.
PACS: 78.67.Sc; 82.35Np

INTRODUCTION

The polymer composites with semiconductor nano-particles have the wide physic-mechanical characteristics and high electro-active properties. Characteristics are caused by polymer matrix and properties are supplied by corresponding fillers [1,2]. The development of new compositions on their base has the practical interest at manufactoring of high-sensitive selective chemical sensors and photo-luminescent transformers [3-7]. The modification procedure of polymers by crazing method in liquid medium has big possibilities among different methods of nano-composite obtaining [8-10].

Earlier we have investigated the nano-composite electric properties on the base of low-density polyethylene (LDPE) and cuprum sulfide (CuS) obtained by crazing method of polymer in active liquid medium [11,12]. The aim of the presented work is the study of LDPE/CdS nano-composite electric properties formed on the base of LDPE films previously modified by γ-irradiation action.

EXPERIMENTAL PART

The γ- irradiation of LDPE up to dose 500 kGy is carried out in installation PXM-γ-25M on the base of Co^{60} isotope. The measurements of ρ_v volume resistivity are carried out with the help of teraohmmeter E6-13A at sample linear temperature growth with velocity ~2,5 K/min.

The orientation stretching of polymer samples LDPE is carried out in isopropanol-water medium with the help of devices developed by authors [11]. The unit elongation of vane-form part of irradiated sample films at nano-particle formation is 10-30% in dependence on irradiation dose. CdS nano-particle in oriented polymer matrix LDPE are formed from CdCl and Na_2S salt solutions at different component concentrations. CdS nano-particles are formed in pores formed at oriented stretching of polymer films by layerwise chemisorption ion method. In formation process the sulfur ion sorption are firstly carried out and then cadmium ion sorption is carried out after film intermediate washing by distilled water. By this fact the one cycle of CdS nano-particle formation in forming pores is ended. One can regulate the sizes and quantity of formed CdS nano-particles in polymer film pores changing the number and time of the cycles. The composite samples with 6 CdS formation cycles by 30 min duration each one are used in the investigations. CdS nano-particle formation is observed by film color change after each sorption cycle. CdS nano-particle number in polymer matrix is defined by weight method and it is ~ 2,7% vol. for investigated samples with six formation cycles.

EXPERIMENTAL RESULTS AND THEIR DISCUSSION

The comparison of temperature dependences of resistivity $lg\rho_v=f(1/T)$ of LDPE/CdS (fig.1) composite samples shows that slope ratio of dependences for composite formed on the base of irradiated film is bigger than corresponding slope of ratio for composite on the base of` initial film.

Such dependence motion means that $\boldsymbol{E_a}$ conduction activation energy for composites on the base of irradiated films is bigger than one for composites on the base of unirradiated films that is the result of formation of new relatively deep trap centers. As it is seen from fig. 1, the composite samples formed on the base of LDPE irradiated films have the cavity on $lg\rho_v=f(1/T)$ dependences in low-temperature region (curve1) which decreases in composites of irradiated LDPE (curve 2; 100kGy) and disappears (curves 3,4; 300 kGy and 500kGy). By our opinion, the observable cavity is the result of moisture desorption sorbed at preparation and saving of composite samples. At influence of previous irradiation by low doses the stitching processes dominate. These processes worse the pore-formation at oriented stretching of polymer matrix and moisture sorption. The polymer matrix destruction processes dominate at influence of previous irradiation by high doses in volume but stitching processes continue on surface [13]. We propose that stitching preventing the moisture sorption and formed polymer active centers interacting by formed nano-particles lead to relative increase of composite resistance (curves 3,4 on fig.1).

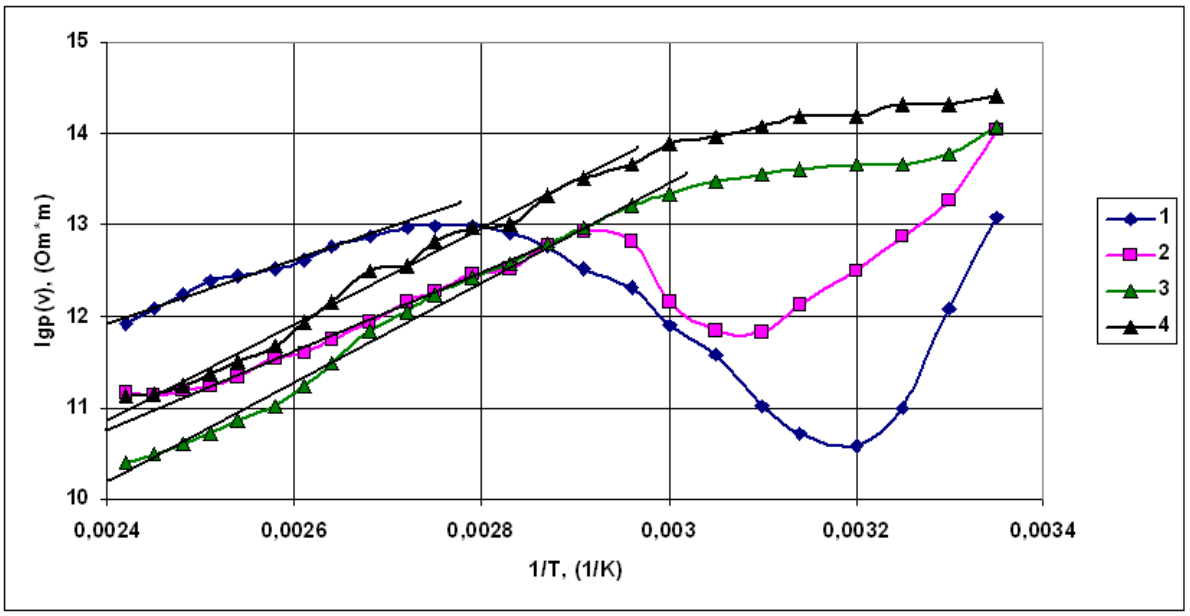

Fig.1. Temperature dependences of resistivity of LDPE/CdS nano-composites formed on the base of previously γ-irradiated LDPE at different doses; 1- D = 0; 2 – D = 100kQr; 3 – D = 300 kQr; 4 – D = 500kQr

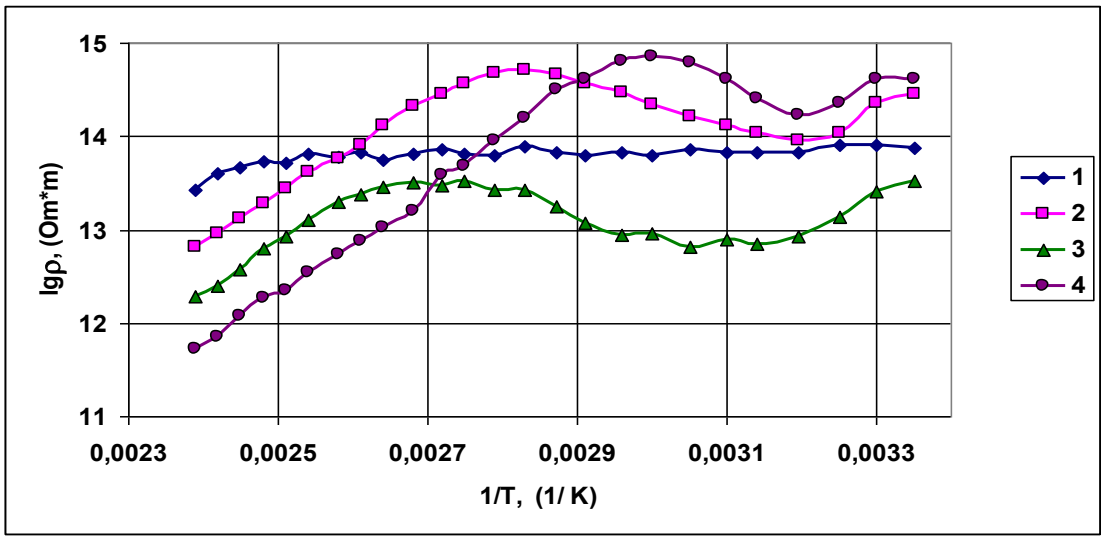

Fig. 2. Temperature dependences of resistivity of LDPE/CdS nano-composite pressed after formation: 1- initial.; 2- 100kGy; 3- 300kGy; 4- 500kGy.

The polymer destruction results in high-temperature region are expressed by increase of dependence inclination with increase of γ-irradiation dose.

The composite thermotreatment is carried out by thermal pressing method with the aim of obtained structure perfection and composite parameter stabilization. The thermal dependences $lg\rho_v=f(1/T)$ of resistivity of LDPE/CdS composite samples formed on the base of irradiated LDPE which are treated by thermotreatment by short temporary thermal pressing during 5 minutes at polymer matrix melting point, are shown on fig.2.

It is seen that enough strong radiation influence is observed in spite of thermotreatment of samples by pressing. The beginning of high-temperature part decay shifts to the side of low temperatures (heat resistance worsens) with increase of matrix previous irradiation dose but angle of inclination of resistance decay doesn't change. It is considered that thermotreatment of LDPE/CdS nano-composites formed on the base of γ-modified polymers leads to stabilization of structural and energy states of capture carrier active centers formed by polymer previous irradiation.

At the thermotreatment the nano-particles formed on subsurface area penetrate into sample volume and as a result the surface active centers (energy state) leading to activation energy change disappear and its value stabilizes. Moreover, during thermotreatment the oxidation of separate chain links previously radiated polyethylene by the way of linking of formed radicals with oxygen takes place in the presence of oxygen.

The oxidation causes the additional destructions and polymer chain shortening decreasing its molecular mass and increasing its mobility and concentration [13]. As it

was above mentioned, this is accompanied by shifting of decay beginning to the side of low temperatures.

Thus, the observable changes in $\rho_v=f(1/T)$ nano-composite dependences on the base of LDPE with modification different doses by previous γ-irradiation are result of difference of molecular segment mobility of crazed oriented regions and difference of radiation process velocities in the structure of oriented polymer matrix. The introduction of CdS nano-filler in LDPE by polymer crazing method changes the molecular segments mobility and ipso facto causes the effective radiation modification of low-density polyethylene.

Thermotreatment of HDPE/CdS nano-composites formed on the base of γ-modified polymers leads to stabilization of structural and energy states because of filler penetration in matrix volume.

The thermal oxidation of polymer matrix decreasing the molecular mass and increasing its mobility and concentration, lead to change of their electric conduction.

[1] *N. Pak, A.N. Levkin.* Izv. RGPU. №10(64). Nauchniy jurnal: Estestvennie i tochnie nauki. 2008. s. 74–85 (in Russian).

[2] *A.A. Richkov, A.A. Maligin, S.A. Trifonov, D.A. Richkov.* Jurnal prikladnoy khimii. 2004. t.77. Vip. 2, s. 280–284. (in Russian).

[3] *A.A. Biryukov, E.Yu. Gotovcheva, T.I. Izaak, V.A. Svetlichniy.* Vestnik Tomskoqo qosudarstvennoqo universiteta. 2013. № 375. s. 194. (in Russian).

[4] *E.I. Grigorev, S.A. Zavyalov, S.N. Chvalun.* Jur. Rossiyskie nanotekhnologii, t.1, № 1-2, 2006, s.58-70. (in Russian).

[5] *M.R. Stasenko, T.V. Semenistaya.* Izvestiya YuFU, tekhn. nauki. 2013, №8, s.166 -172. (in Russian).

[6] *M.B. Muradov, M.A. Nuriev, G.M. Eivazova.* Sensitivity of Composites Based on Gelatin and NanoparticlesCu2S and CdS to Vapors of Some Organic Compounds, Surface Engineering and Applied Electrochemistry, 2007, Vol. 43, No. 6, pp. 512–515.

[7] *N.C. Greenham, X. Peng, A.P. Alivisatos.* Phys.Rev. B. 1996, v. 54, n. 24, p. 17628–17637.

[8] *A.L. Volynskii, N.F. Bakeev.* Solvent Crazing of Polymers. Amsterdam; New York; Tokyo; Elsevier, 1995, p. 410.

[9] *A.L. Volinskiy, N.F. Bakeev, E.Q. Rukhlya, L.M. Yarisheva.* Jur. Rossiyskie nanotekhnologii, 2007, t.2, № 5-6, s.44-55. (in Russian).

[10] *V.I. Kodolov, N.V. Khokhryakov, V.V. Trineeva, I.I. Blagodatskikh.* Khimicheskaya fizika i mezoskopiya. 2008, tom 10, №4, s. 448-460. (in Russian).

[11] *A.M. Maharramov, M.A. Nuriev, A.A. Shukyurova.* Jur. Plasticheskie massi, 2012, № 10, c. .9-11. (in Russian).

[12] *M.A. Nuriyev, A.M. Maharramov, A.A. Shukurova, I.M. Nuruyev.* Electrical Properties of PELD-CdS Nanocomposites Based on Pre-Irradiated Polymers. Inter. Konf. "Nuclear Science and its Application", Samarkand, Uzbekistan, 25-28 September, 2012, p. 204-206.

[13] *N.V. Jilkina, Yu.T. Larin, V.M. Vorobev.* Nauka i texnika, 2004, № 3 (286), c. 11-15. (in Russian).

Received: 16.09.2014

ISSN 1028-8546

2014, Vol. XX, № 4
Section: En

CONTENTS